2011

Experimental assessments of intrafractional prostate motion on radiation boosts to a dominant intra-prostatic cancer lesion

Ady Kamel Abdellatif

Experimental assessments of intrafractional prostate motion on radiation boosts to a dominant intra-prostatic cancer lesion

(Spine title: Radiation Boosts to a Dominant Intra-prostatic Cancer Lesion)

(Thesis format: Integrated-Article)

By

Ady K. Abdellatif

Graduate Program in Physics

A thesis submitted in partial fulfillment of the requirements for a degree of

Master of Science

The School of Graduate and Postdoctoral Studies

The University of Western Ontario

London, Ontario, Canada

THE UNIVERSITY OF WESTERN ONTARIO
SCHOOL OF GRADUATE AND POSTDOCTORAL STUDIES

CERTIFICATE OF EXAMINATION

Supervisor

Dr. Eugene Wong

Supervisory Committee

Dr. Jeff Chen

Dr. Jerry Battista

Dr. Glenn Bauman

Examiners

Dr. Aaron Fenster

Dr. Blaine Chronik

Dr. Stewart Gaede

The thesis by

Ady Kamel Abdellatif

entitled:

Experimental assessments of intrafractional prostate motion on radiation boosts to a dominant intra-prostatic cancer lesion

is accepted in partial fulfillment of the
requirements for the degree of
Master of Science

Date_____

Chair of the Thesis Examination Board

Abstract and Keywords

Abstract:

We investigated the impact of intrafractional prostate motion on radiation dose distributions to the whole prostate with boosts to a dominant intra-prostatic cancer lesion (DIL) from sequential boost plans (separate prostate and boost plans) and simultaneous boost plans (single prostate and boost plan).

Six treatment plans were generated for two patient CT scans. Plans were delivered and 2D dose distributions were measured on a phantom using a motion platform driven with typical prostate intrafractional motions.

The relative root mean square difference between measured dose with and without motion inside the DIL for the simultaneous plans (1.6%–2.1%) were lower than those for the sequential plans (4.5%–7.2%) and the total beam-on time was shorter. Dose escalation to DIL using simultaneous boost plans with sufficient margin around DIL (7 mm) is feasible provided that severe prostate motion is infrequent (< 5/35 fractions).

Keywords: Intensity Modulated Radiation Therapy, Volumetric Modulated Arc Therapy, Dominant Intra-prostatic Lesion, Prostate Cancer, Prostate Intrafractional Motion.

Co-Authorship

Chapter 2 of this thesis is co-authored by the following individuals:

Ady Abdellatif: performed the treatment planning, motion platform programming, delivered treatment plans, analyzed the data and wrote the manuscript.

Jeff Craig: wrote the code used to rotate the treatment plans and helped writing some codes used for data analysis.

Michael Jensen: wrote the gamma code used for data analysis.

Matt Mulligan: assisted with treatment planning and delivery.

Homeira Mosalaei: assisted with treatment planning and delivery.

Glenn Bauman: oversaw project, provided assistance and guidance for analysis and presentation of data.

Jeff Chen: oversaw entire project, assisted with treatment planning, treatment delivery and provided assistance and guidance in terms of experimental methods, data analysis and presentation of data.

Eugene Wong: oversaw entire project, assisted with treatment planning and provided assistance and guidance in terms of experimental methods, data analysis and presentation of data.

Dedicated to the love of my life, Zain.

Your love, support and encouragement made the last part of this journey endurable.

I love you, forever and always.

Acknowledgements

First, I would like to thank my parents, Kamel and Daad. You have always believed in me, you have always supported and encouraged me to follow whatever path I choose for myself. Without you I would have never fulfilled any of my dreams in life. I love you both. I will not forget the support and encouragement of my two sisters, Sahar and Ruba. Their endless love was a huge motivation for me to take this huge step in changing my career to medical physics.

I would like to thank my supervisor Eugene Wong for the great opportunity he offered me. I will never forget this favour all my life. Naturally, the guidance you provided me with and the discussions we had were invaluable. I consider myself quite fortunate to have been able to work with such an experienced, patient, and considerable scientist.

I owe special thanks to Jeff Chen. His continuous help and assistance whenever I needed is extremely appreciable. You were always available for me whenever I needed help no matter how busy you were. You are definitely my mentor for life.

I would like to thank Matt Mulligan and Homeira Mosalaei for the great training they offered me throughout the two years of my masters. Without the two of you I would have been totally lost.

Thank you to the entire physics department at the London Regional Cancer Program. This group of people is the friendliest, most experienced and most professional group I have ever worked with. Special thanks to my committee members Jerry Battista and Glenn Bauman. Your input, suggestions and questions led me always to expand my

investigations to new areas. I would like also to thank Stewart Gaede and John Taylor for their assistance with the CT scans I needed to finish this project.

Thanks to Ms. Marnie Adams for lending me her laptop near the end of this project after the breakage of my personal laptop.

Finally, I would like to thank the awesome 4th floor physics group. Their professional assistance and the brain storming sessions we had were amazing. Thanks to Jeff Craig for his assistance and help in teaching me MATLAB coding, thanks to Dave Turnbull for sharing his expertise with me. Thank you Brandon, Jeff, Carol, Timothy and Bryan for the great friendship and for the invaluable knowledge you provided me with. Thanks to Bon Ryu, Nikolaj Jensen, Michael Jensen and Doug Hoover for sharing their knowledge with me and for their positive discussions during out weekly meetings.

I am grateful to the Canadian Institutes of Health Research for the financial support of this research. I am also grateful for the scholarship awards of the University of Western Ontario.

Table of Contents

List of Tables

List of Figures

List of Abbreviations

2D	Two Dimensional
3D	Three Dimensional
AAPM	American Association of Physicists in Medicine
CBCT	Cone Beam Computed Tomography
CIHR	Canadian Institutes for Health Research
CT	Computed Tomography
CTV	Clinical Target Volume
DIL	Dominant Intra-prostatic Lesion
DVH	Dose Volume Histogram
EBRT	External Beam Radiation Therapy
fx	Fraction
GTV	Gross Target Volume
Gy	Gray, unit of dose
ICRU	International Commission on Radiation Units
IGRT	Image Guided Radiation Therapy
IMRT	Intensity Modulated Radiation Therapy
LINAC	Linear Accelerator
MLC	Multileaf Collimator
MRI	Magnetic Resonance Imaging
MV	Megavolts
OAR	Organ At Risk
OICR	Ontario Institute for Cancer Research
PET	Positron Emission Tomography
PTV	Planning Target Volume
rrms	Relative root mean square
RTOG	Radiation Therapy Oncology Group
SPECT	Single Photon Emission Computed Tomography
TPS	Treatment Planning System
VMAT	Volumetric Modulated Arc Therapy

CHAPTER 1

Introduction

1.1 Cancer

Cancer is the class of diseases in which a cell or a group of malignant mass of cells displays uncontrolled growth. Uncontrolled growth of cells is not lethal; it is the interference of the uncontrolled growth with the normal function of critical organs and act negatively on the survival of the subject [1]. Prostate cancer starts in the cells of the prostate gland and it is the most common cancer in Canadian men. In 2010 an estimated 24,600 men will be diagnosed with prostate cancer and 4,300 will die of it [2].

There are three main techniques to treat prostate cancer. These techniques are surgery, chemotherapy and radiation therapy. Typically combinations of these techniques are used to maximize the chances of curing the patient. There are considerable side effects for each of these techniques; surgery involves the removal of the prostate which results in total loss of its functionality. Chemotherapy can result is serious side effect such as feeling nauseous, lack of energy and hair loss [3]. Radiation therapy side effects can include urological and rectal bleeding [4]. Unlike surgery and chemotherapy, with accurate and precise radiation treatment delivery some of these side effects can be avoided. Radiation therapy is the focus of this work.

1.2 Radiation Therapy

Radiation therapy is the clinical process that uses radiation in the treatment of cancer. This can be achieved by using ionizing radiation to control cancerous masses

within the body. The aim of radiation therapy is to deliver a very accurate dose of radiation to a well-defined target volume with minimal damage to surrounding normal tissue, resulting in eradication of the disease, the prolongation of life and/or the improvement in the quality of life [5]. Radiation can be delivered in two ways, externally using a medical linear accelerator (external beam radiation therapy (EBRT)) or internally by implanting radioactive seeds surgically in an organ such as the prostate (Brachytherapy). The amount of radiation delivered to a target is expressed in units of Gray, Gy (J/kg).

1.2.1 The Linear Accelerator

Medical linear accelerators (LINACs) have become the predominant machine used in the treatment of cancer with ionizing radiation. LINACs provide electron beams with several electron energies (6, 9, 12, 16, 20 MeV) as well as photon beams with energies (6, 10, 18 MV) [6]. Simply the electrons, generated by an electron gun, are accelerated in a linear trajectory in a waveguide, then once they reach the head of the machine they follow a 270° trajectory using a bending magnet. As shown in Figure 1.1 [6], the electron beam will travel through an ion-chamber and may follow one of two tracks, if an electron beam is to be used then the electron will hit a scattering foil and if a photon beam is to be used then the electrons will hit an X-ray target and bremsstrahlung photon radiation will be produced.

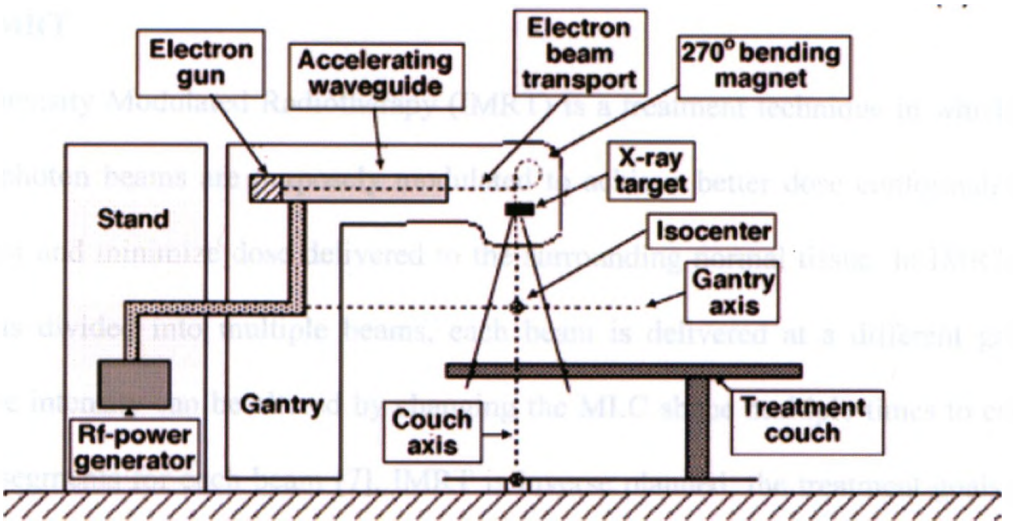

Figure 1.1. A schematic diagram of the major components of a medical linear accelerator. (taken from Figure 3.11b of Podgorasak 2006 [6])

The beam then passes through a two stage collimating system, the first system is jaws and the second is the multileaf collimator (MLC). The jaws consist of two pairs of blocks made of a high atomic number material such as lead to maximize attenuation. The jaws can shape the beam into square or rectangular shapes up to 40 cm wide. The MLC, shown in Figure 1.2, consists of a number of leaves (typically 120 and usually made of tungsten). Each leaf is controlled by an individual computer-controlled motor. The MLC provides a rapid way of creating an irregular field shapes.

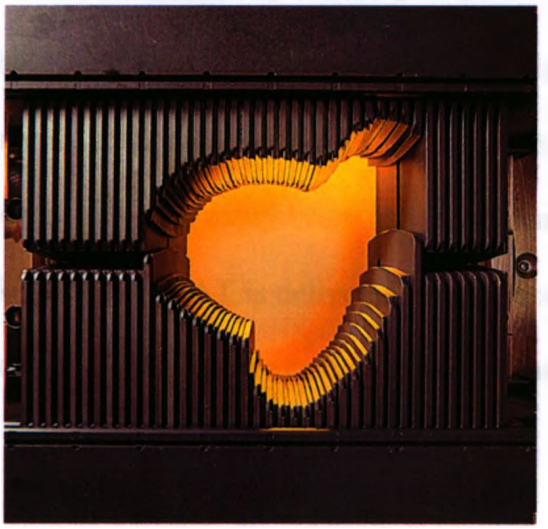

Figure 1.2. An image showing a 120 leaves MLC (adapted from VARIAN Medical Systems, Palo Alto, California, USA).

1.2.2 IMRT

Intensity Modulated Radiotherapy (IMRT) is a treatment technique in which the incident photon beams are purposely modulated to achieve better dose conformality to the tumour and minimize dose delivered to the surrounding normal tissue. In IMRT the delivery is divided into multiple beams, each beam is delivered at a different gantry angle. The intensity can be altered by changing the MLC shape multiple times to create multiple segments for each beam [7]. IMRT is inverse planned; the treatment goals and objectives are given to the treatment planning software, which will try to find the set of beam shapes and intensities that will achieve these goals.

1.2.3 VMAT

Volumetric Modulated Arc Therapy (VMAT) is recent treatment technique [8-9]. In general, arc therapy is the type of radiation treatment that includes the delivery of radiation while the gantry is rotated around the patient. A VMAT plan usually consists of one or two arcs or more delivering continuous radiation to the patient. During delivery the gantry changes speed, the MLC changes shapes and the dose is delivered at different rates. VMAT is also inverse planned. One of the advantages of VMAT over IMRT is that the entrance dose to the patient gets distributed since the dose is delivered from all angles not just from 5 or 7 angles as in IMRT. Another advantage for VMAT is delivery time, in IMRT the gantry has to be moved to the new position for every beam and the system tests the new parameters for every beam. Unlike IMRT, VMAT is delivered in one setup and the system needs to test the parameters once only which improves the treatment time.

VMAT is a fairly new treatment technique and it has yet to be implemented clinically in many treatment facilities. It requires the implantation of new protocols and new quality assurance strategies.

1.2.4 Monitor Units and Control Points

A monitor unit (MU) is a measure of the machine output from a set of ion chambers in a linear accelerator in radiation therapy. Linear accelerators are calibrated such that 1 MU gives an absorbed dose of 1 cGy delivered in a water phantom at 5 cm depth on the central beam axis for both 6 an 18 MV when irradiated with a 10×10 cm^2 field at a source to surface distance (SSD) of 95 cm [10]. In general, the primary ionization chamber in the linear accelerator measures MUs, once the operator preset number of MUs has been reached, the primary ionization chamber circuitry shuts the LINAC down and terminates the dose delivery to the patient.

Control points (segments) represent points at which certain parameters for dose delivery are determined. These parameters include MLC positions and fractional MUs to be delivered at this particular MLC shape. For IMRT, each beam consists of several segments and during beam delivery the beam switches off after the delivery of the MUs assigned for that particular segment and the MLCs move to the new shape for the following segment and the beam is switched on again. This delivery concept is called step and shoot. As for VMAT, the arc is divided into angular control points. While the gantry is moving between control points the MLCs change shape and the fractional MUs assigned for the first control point is delivered. Once the delivery is over and the gantry is

at the next control point, the MLCs will be at positions assigned for that particular control point.

1.3 Intrafractional Motion

Motion of the prostate during each fraction of EBRT is referred to as intrafractional motion. Example of intrafractional motion is lung motion (breathing) and prostate motion during treatment. For the prostate these variations depend on the bladder and rectum fillings [11]. A study [12] provided continuous, real-time localization and monitoring of the prostate. The study reported different prostate motion patterns during the delivery of radiation therapy. Depending on the motion pattern, prostate can move anywhere between 1 to 15 mm. This can result in missing the tumour and increased irradiation of parts of the rectum and bladder.

1.4 Radiation Therapy treatment process

The process starts with the patient being diagnosed with cancer. The oncology team then decides on the treatment strategy to be implemented. If radiation therapy is the choice of treatment then the patient is sent for medical imaging to determine the location and size of the tumor [13]. Before the patient is treated, the radiation oncology team must make a decision on four inter-related factors: (1) goal of treatment outcome, (2) volume to be treated, (3) Radiation treatment technique and (4) dose to be delivered [14]. The details of the process are described in the following subsections.

1.4.1 Patient Imaging

A Computed Tomography (CT) scan is usually used for patient imaging. This is because CT provides electron density information which governs the probability of radiation interactions with the imaged structure. This can be accompanied by other imaging modalities such as magnetic resonance imaging (MRI), single photon emission computed tomography (SPECT) or positron emission tomography (PET). These techniques can be used to provide information not visualized using CT scans such as hypoxic regions within the affected area or better visualization of tumor and surrounding tissues.

1.4.2 Target Definition

The protocol that defines the treatment target is set laid out in the International Commission on Radiation Units Report (ICRU-62) [15]. It describes several target and critical structure volumes that are required for the treatment planning process and used for the plan evaluation. These volumes are contoured on the patient CT scans by a radiation oncologist. The principal volumes related to 3D treatment planning are the gross target volume (GTV), the clinical target volume (CTV), the internal target volume (ITV) and the planning target volume (PTV). Figure 1.3 shows the four volumes and how they are related to each other.

The GTV is defined as the visible extent of the malignant disease which is based on the information provided by different imaging modalities. The microscopic disease spread around the GTV that is invisible on the CT images can be accounted for by expanding the GTV into the CTV. The ITV consists of the CTV plus a margin and it

accounts for intrafractional motion resulting from organ motion during treatment. A setup margin is added to the ITV to create the PTV to account for setup uncertainties. If there is no ITV, the CTV is directly expanded to the PTV to account for both intrafractional motion and setup uncertainties.

Other organs that are in the vicinity of the CTV are contoured to ensure that they are not irradiated to levels that will induce toxicities. These organs are called organs at risk (OARs).

In the case of prostate cancer, the prostate is the CTV since the prostate will include both the gross and microscopic spread of the disease. The bladder, the rectum, and the femoral heads are considered OARs.

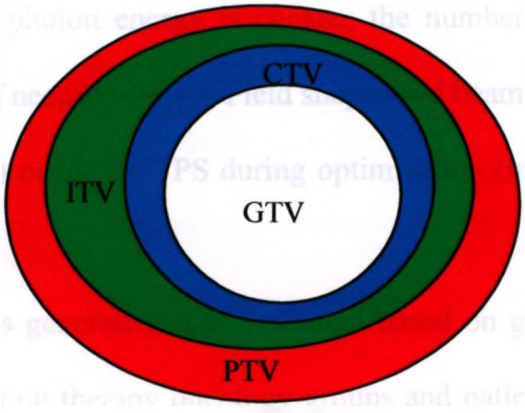

Figure 1.3. A diagram shows the four volumes of interest for treatment planning, the GTV, The CTV, the ITV and the PTV as set by the ICRU-62.

1.4.3 Treatment Planning

Once the target volumes and OARs are identified and delineated, the radiation oncology team uses set guidelines, protocols, and clinical experience to make a decision about the prescription dose and fractionation plan [13]. Since cancerous cells response to

ionizing radiation is different from normal tissue cells, the dose is prescribed to be given in fractions, typically 2 Gy per fraction for 5 – 7 weeks [13].

A treatment planning system (TPS) is used to generate the treatment plan using the medical images and the contours created by the radiation oncologist. This is the stage were all the radiation treatment techniques are evaluated. Techniques include using multiple static beams that are planned in a forward or inverse manner to less common techniques like tomotherapy and arc therapy.

The treatment plan starts by choosing a plan isocenter, which is the point at which all the beams will intersect, and is usually the center of the target. The next step is to choose the photon energy. The depth of the maximum dose depends on the energy of the beam and is directly proportional to it. Figure 1.4 shows the depth-dose diagrams for photons [6]. Once the photon energy is chosen, the number of beams, energy, beam angles and modifiers (if needed) are set. Field shapes and beam weights are chosen by the user (forward planning) or by the TPS during optimization (inverse planning), followed by dose calculation.

After the plan is generated, it is evaluated based on guidelines set by treatment protocols, certain radiation therapy oncology groups and patient-specific considerations. These guidelines provide the OARs normal tissue tolerances and the PTVs dose limits. For example, one of the constraints on prostate plans is for the PTV to receive at least 95% of the prescribed dose for the plan to be considered acceptable [17]. Dose volume histograms (DVHs) represent a unique dose evaluation tool that is frequently used in radiation therapy [16].

DVHs can be represented in two forms, differential and integrated. The differential DVH represents a histogram of the sum of the number of voxels with an average dose within a certain dose range and plots the resulting volume as a function of dose for a target structure or an OAR. An integrated DVH represents the fractional normalized volume receiving at least a dose *D* plotted against dose [10].

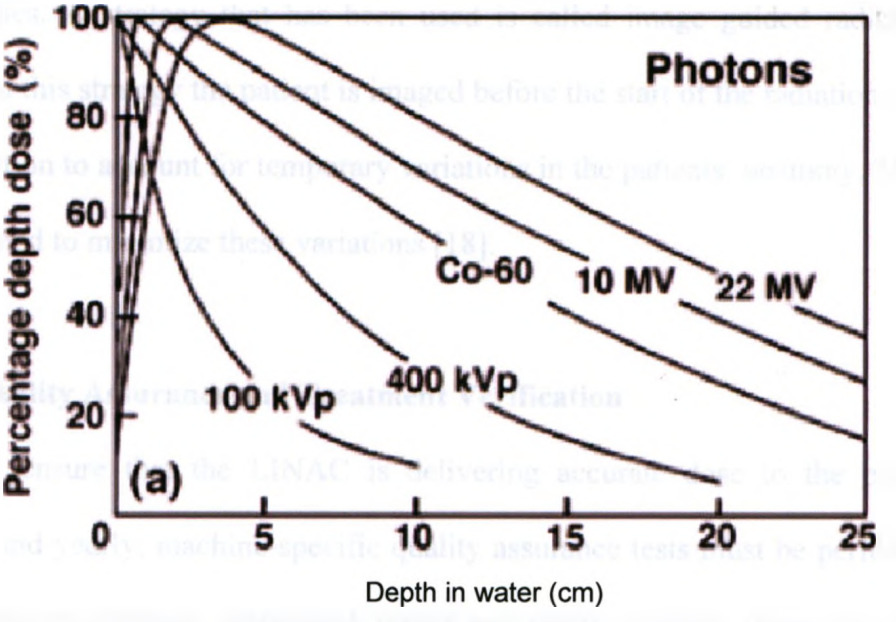

Figure 1.4. The depth-dose diagrams for photons. (taken from Figure 1.2 of Podgorasak 2006 [6])

1.4.4 Treatment Delivery

Once the treatment plan is generated, it will be imported to information management software to verify if the plan is compatible with the machine delivery constraints. Once the plan is verified and scheduled it will be tested for quality assurance (see section 1.4.5). The plan is delivered over many fractions and the total dose delivered is the accumulative dose delivered over the course of all the fractions. Uncertainties in the position and shape of the GTV are present at each fraction. These uncertainties can be

due to interfraction effects (changes between treatment and planning) and intrafraction effects.

Interfraction effects result from day-to-day patient setup variations, variations in the filling of bladder and rectum, weight loss or gain and the reduction of the GTV volume as an outcome of the treatment. Expanding the CTV to PTV covers all of these uncertainties. A strategy that has been used is called image guided radiation therapy (IGRT). In this strategy the patient is imaged before the start of the radiation treatment on every fraction to account for temporary variations in the patients' anatomy. The patient is then adjusted to minimize these variations [18].

1.4.5 Quality Assurance and Treatment Verification

To ensure that the LINAC is delivering accurate dose to the patient, daily, monthly, and yearly, machine-specific quality assurance tests must be performed. These tests include mechanical, operational, output and safety systems. These tests are outlined in documents such as AAPM TG-40 [19].

There are several tools to use for treatment patient-specific plan delivery verification. These tools involve films [20], diode arrays such as MapCheck™ (Sun Nuclear Corporation) [21] and ion chamber arrays such as the PTW 2D-Array Seven29 [22]. Before a plan is delivered to a patient, one of these tools is used to verify the quality of the plan by comparing the measured dose in a plane to the same calculated dose on the same plane, a technique that is used to evaluate that is called the Gamma analysis technique.

1.4.5.1 Gamma Analysis Technique

The Gamma analysis technique is a technique used for quantitative comparisons between measured and calculated dose distributions. Two thresholds are used as comparison parameters, the dose-difference (ΔD) and the distance-to-agreement (Δd). The thresholds represent tolerances in the error of the dose and distance to agreement in regions of low and high dose gradients, respectively.

For the dose difference criteria, difference between the measured and calculated doses are computed. The distance to agreement is the distance between a measured data point and the nearest point in the calculated dose distribution that exhibits the same dose. The dose difference and distance to agreement evaluations complement each other when used as determinants of dose distribution calculation quality [23].

The Gamma analysis technique simultaneously incorporates the dose and distance criteria. It provides a numerical quality index that serves as a measure of disagreement in the regions that fail the acceptance criteria and indicates the calculation quality in regions that pass. For a single measurement, the Gamma value is defined as

$$\gamma(r_m) = \{\min \Gamma(r_m, r_c)\} \forall \{r_c\} \quad (1)$$

where

$$\Gamma(r_m, r_c) = \sqrt{\left(\frac{D_m(r_m) - D_c(r_c)}{\Delta D}\right)^2 + \left(\frac{r_m - r_c}{\Delta d}\right)^2} \quad (2)$$

$D_m(r_m)$ is the measured dose at position r_m and $D_c(r_c)$ is the calculated dose at position r_c. The does difference and distance to agreement criteria therefore become

$\gamma(r_m) \leq 1$, if dose difference and distance to agreement are less than the respective thresholds,

$\gamma(r_m) > 1$, if dose difference and distance to agreement are less than the respective thresholds,

In the clinic, we accept a treatment plan when the difference from measurements yielded $\gamma(r_m) \leq 1$ in at least 90% of the points.

1.4.6 Set-up Verification with IGRT

Before each treatment, patients are aligned on the LINAC couch using external marks (tattoos) made during their planning CT and room lasers. However, we can improve the setup and reduce the PTV margin if we can visualize patient's internal anatomy and/or tumor. Pre-treatment imaging of the patient allows for the correction of these set-up errors.

It is currently possible to image patient anatomy just before delivery of a fraction of radiotherapy, thus gaining precise knowledge of the location of the target volume on a daily basis. This technique of dose delivery to the patient is known as IGRT and it ensures that the relative positions of the target volume and some reference point for each fraction are the same as in the treatment plan. This may allow reduced treatment margins, fewer complications, dose escalation and the avoidance of geographical misses. The ideal image guided system will allow the acquisition of soft tissue images at the time of each fraction of radiotherapy [10].

Several IGRT systems are currently commercially available. All systems allow pre-treatment imaging immediately after a patient is positioned on the LINAC treatment

table for therapy. VARIAN IGRT system (VARIAN Medical Systems, Palo Alto, California, USA) is based on direct integration of a kilovoltage or/and megavoltage imaging system with an isocentric medical LINAC, allowing the acquisition of Cone Beam CT (CBCT)". The kilovoltage system consists of a conventional X-ray tube mounted on a retractable arm at 90° to the high energy treatment beam and a flat panel X-ray detector mounted on a retractable arm opposite the X-ray tube [24].

kV CBCT imaging enables visualization of the tumour location just prior to patient treatment on a LINAC. The technique integrates CT imaging with a LINAC and involves acquiring multiple planar images produced by a kilovoltage cone beam rotating a 180° or 360° about the patient in the treatment position on the LINAC couch. The acquired data are then compared with the planning CT data and a decision is made on adjusting the patient position to account for tumour motion or set-up error.

1.5 Motivation

Escalating the dose to the whole prostate can expose the bladder and rectum to dose that exceeds normal tissue tolerances. Enabling dose escalation to the dominant intraprostatic lesion (DIL) that requires a higher dose than the remainder of the prostate without exceeding normal tissue tolerances is a motivation of this study. With the advances in functional imaging technology identifying DIL is now possible [25-32].

However, intrafractional motion can affect the outcome of treatment considerably. With IGRT, intrafractional motion is minimized. Previous studies on dose escalation to a DIL involved treatment planning studies and delivery without considering the effect of intrafractional motion [33-36]. On the other hand, a number of studies have computer

simulations investigating the impact of inter- and intra- fraction prostate motion on the dose distributions [37-40]. Investigating the effect of intrafractional motion on the delivery of the generated treatment plans is a second motivation for this study.

1.6 Hypothesis

The hypothesis of this thesis is as follows: "there exists a dose escalation to a DIL treatment plan that is insensitive to prostate intrafractional motion". This plan can be an IMRT plan or a VMAT plan or combination of both. The plan can be simultaneous (one plan) or sequential (two plans). Sequential plans are divided into a plan for the DIL and a plan for the prostate. We seek a plan that can be delivered with no intrafractional motion management and still have high chance in delivering the prescribed dose to 95% of the PTV. This would allow the treatment of prostate cancer patients minimizing the need to have real-time monitoring of the prostate motion during treatment. This is the first experimental phantom study that assesses the impact of prostate intrafractional motion on the delivery of different treatment plans.

1.7 Thesis Overview

This thesis is divided into three chapters. Chapter 1 is a general introduction to cancer and prostate cancer. It includes a general overview of the radiation therapy treatment process that covers the different radiation therapy treatment techniques used in this study. Chapter 2 is an adaptation of a manuscript that will be submitted to the Medical Physics journal. This work has been presented locally (London, Ontario, Canada) at the University of Western Ontario Department of Oncology Research and

Education Day (June 2009 and 2010), CHIR Team Grant & OICR Imaging Pipeline Platform "Imaging Applications in Prostate Cancer" (November 2010) and at the American Association of Physicists in Medicine annual conference in Philadelphia, Pennsylvania, USA (July 2010). This chapter introduces an experiment that assesses the effect of the prostate intrafractional motion on the delivery of the dose escalation treatment plans to a DIL. Six treatment plans per patient were generated and delivered on a phantom with no motion applied. Six motion patterns were programmed on a commercial motion platform. The generated plans were then delivered to the phantom after the motion platform is set in motion. The measured data is analyzed and the results are compared for the different plans. This chapter includes more figures and more details than the submitted manuscript. Chapter 3 includes the discussion of the results listed in Chapter 2 in addition to the conclusions, limitations and future work.

1.8 References

1. Stevens A and Lowe J. Neoplasia. In: Pathology, Mosby. Edinburgh: 2000 p. 79-105.

2. Canadian Cancer Statistics. Canadian Cancer Society, 2010.

3. Chemotherapy: A guide for people with cancer. Canadian Cancer Society, May 2009.

4. Radiation Therapy: A guide for people with cancer. Canadian Cancer Society, May 2009.

5. Van Dyk J. The modern technology of radiation oncology. Medical Physics Publishing; 1999.

6. Podgorsak EB. Radiation Physics for Medical Physicists. Heidelbergy; Springer-Verlag; 2006.

7. Teh B, Amosson C, Mai W. Intensity modulated radiation therapy (IMRT) in the management of prostate cancer. Cancer Invest 2004;22(6):913–924.

8. Yu C. Intensity modulated arc therapy with dynamic multileaf collimation: an alternative to tomotherapy. *Phys. Med. Biol.* 1995;40:1435.

9. Otto K. 2008 Volumetric modulated arc therapy: IMRT in a single gantry arc. *Med Phys.* 2007;35:310–317.

10. Podgorsak EB. Radiation Oncology Physics: A Handbook for Teachers and Students. Vienna, Austria; IAEA; 2005.

11. Willoughby TR, Kupelian PA, Pouliot J, *et al.* Target localization and real-time tracking using the Calypso 4D localization system in patients with localized prostate cancer. *Int. J. Radiation Oncology Biol. Phys* 2006;65:528–534.

12. Kupelian PA, Willoughby TR, Mahadevan A, *et al.* Multi-institutional clinical experience with the Calypso system in localization and continuous, real-tima monitoring of the prostate gland during external radiotherapy. *Int. J. Radiation Oncology Biol. Phys* 2007;67:1088–1098.

13. Van Dyk J. Radiation Oncology Overview. In: Van Dyk J, editor. The modern technology of radiation oncology. Madison (WI): Medical Physics Publishing; 1999. p. 1-17.

14. Halperin EC, Perez CA and Brady LW The Discipline of Radiation Oncology, In: Perez and Brady's Principles and Practices of Radiation Oncology, 5th edition, 2008, p. 1-75.

15. International Commission on Radiation Units and Measurements. ICRU Report 62. Prescribing, recording and reporting photon beam therapy (Supplement to ICRU Report 50). Bethesda, MD: ICRU, 1999.

16. Mohan R, Brewster LJ and Barest GD. A technique for computing dose volume histograms for structure combinations. *Med. Phys.* 1987;14:1048–1052.

17. Radiation Therapy Oncology Group. RTOG 0126. A phase III randomized study of high dose 3D-CRT/IMRT versus standard dose 3D-CRT/IMRT in patients treated for localized prostate cancer. RTOG, 2007.

18. Yan D, Image guided\adaptive radiation therapy, In; New technologies in radiation oncology, Schlegel W., Bortfeld T and Grosu L (editors). Berlin: Springer, p 321-336;2007.

19. Kutcher GJ, Coia L, Gillin M, *et al.* Comprehensive QA for radiation oncology: report of AAPM Radiation Therapy Committee Task Group 40. *Med Phys.* 1994;21:581–618.

20. Sturtewagen E, Fuss M, Paelinck L, *et al.* Multi-dimensional dosimetric verification of stereotactic radiotherapy for uveal melanoma using radiochromic EBT film. *Z Med Phys.* 2008;18(1):27–36.

21. Létourneau D, Gulam M, Yan D, *et al.* Evaluation of a 2D diode array for IMRT quality assurance. *Radiother Oncol.* 2004;70(2):199–206.

22. Spezi E, Angelini AL, Romani F, *et al.* Characterization of a 2D ion chamber array for the verification of radiotherapy treatments. *Phys Med Biol.* 2005;50(14):3361–73.

23. Low D, Harms W, Mutic S, et al. A technique for the quantitative evaluation of dose distributions. Med. Phys. 1998 May;25(5):656–661.

24. Jaffray D, Drake D, Moreau M. A radiologic and tomographic imaging system integrated into a medical linear accelerator for localization of bone and soft-tissue targets. *Int. J. Radiation Oncology Biol. Phys* 1999;45(3):773–789.

25. Groenendaal G, van den Berg CA, Korporaal JG, *et al.* Simultaneous MRI diffusion and perfusion imaging for tumor delineation in prostate cancer patients. *Radiotherapy and Oncology* 2010;95:185–190.

26. Scheidler J, Hricak H, Vigneron DB, *et al.* Prostate cancer: localization with three-dimensional proton MR spectroscopic imaging – clinicopathologic study. *RAD* 1999;213:473–80.

27. Van Dorsten FA, van der Graaf M, Engelbrecht MRW, *et al.* Combined quantitative dynamic contrast-enhanced MR imaging an 1H NMR spectroscopic imaging of human prostate cancer. *J Magn Reson Imaging* 2004;20:279–87.

28. Fütterer JJ, Heijmink SWTPJ, Scheenen TWJ, *et al.* Prostate cancer localization with dynamic contrast-enhanced MR imaging and proton MR spectroscopic imaging. *Radiology* 2006;241:449–58.

29. Hosseinzadeh K, Schwarz SD. Endorectal diffusion-weighted imaging in prostate cancer to differentiate malignant and benign peripheral zone tissue. *J Magn Reson Imaging* 2004;20:654–61.

30. Miao H, Fukatsu H, Ishigaki T. Prostate cancer detection with 3-T MRI: comparison of diffusion-weighted and T2-weighted imaging. *Eur J Radiol* 2007;61:297–302.

31. Park H, Meyer CR, Wood D, Khan A, *et al.* Validation of Automatic Target Volume Definition as Demonstrated for (11)C-Choline PET/CT of Human Prostate Cancer Using Multi Modality Fusion Techniques. *Acad Radiol.* 2010 May;17(5):614–23.

32. Pinkawa M, Attieh C, Piroth MD, *et al.* Dose-escalation using intensity-modulated radiotherapy for prostate cancer – Evaluation of the dose distribution with and without 18F-choline PET-CT detected simultaneous integrated boost. *Radiotherapy and Oncology* 2009;93(2):213-9.

33. Xia P, Pickett B, Vigneault E, *et al.* Forward or intensity planned segmental multileaf collimator IMRT and sequential tomotherapy to treat multiple dominant intraprostatic lesions of prostate cancer to 90 Gy. *Int. J. Radiation Oncology Biol. Phys* 2001;51:244–254.

34. Singh AK, Guion P, Sears-Crouse N, *et al.* Simultaneous integrated boost of biopsy proven, MRI defined dominant intra-prostatic lesions to 95 Gray with IMRT: early results of a phase I NCI study. *Radiation Oncology* 2007;2:36.

35. Shaffer R, Morris WJ, Moiseenko V, *et al.* Volumetric Modulated Arc Therapy and Conventional Intensity-modulated Radiotherapy for Simultaneous Maximal Intraprostatic Boost: a Planning Comparison Study. *Clinical Oncology* 2009;21:401– 407.

36. Pickett B, Vigneault E, Kurhanewicz J, *et al.* Static field intensity modulation to treat a dominant intra-prostatic lesion to 90 Gy compared to seven field 3-dimentsional radiotherapy. *Int. J. Radiation Oncology Biol. Phys* 1999;43:921–929.

37. Craig T, Wong E, Bauman G, *et al.* Impact of geometric uncertainties on evaluation of treatment techniques for prostate cancer. *Int J Radiat Oncol Biol Phys* 2005;62(2):426–36.

38. Maleike D, Unkelbach J, Oelfke U. Simulation and visualization of dose uncertainties due to interfractional organ motion. *Phys Med Biol.* 2006;51(9):2237-52.

39. Hossain S, Xia P, Chuang C, *et al.* Simulated real time image guided intrafraction tracking-delivery for hypofractionated prostate IMRT. *Med Phys.* 2008;35(9):4041–8.

40. Li H, Chetty I, Enke C, *et al.* Dosimetric consequences of intrafraction prostate motion. *Int J Radiat Oncol Biol Phys.* 2008 Jul 1;71(3):801-12.

CHAPTER 2

Experimental assessments of intrafractional prostate motion on sequential and simultaneous boost to a dominant intra-prostatic lesion

This chapter is an adaptation of a manuscript to be submitted to Journal of Medical Physics in 2010, entitled "Experimental assessments of intrafractional prostate motion on sequential and simultaneous boost to a dominant intra-prostatic lesion" by Ady Abdellatif, Jeff Craig, Matt Mulligan, Homeira Mosalaei, Glenn Bauman, Jeff Chen, and Eugene Wong.

2.1 Introduction

Accurate delineation of tumour volume is crucial in external radiation therapy (EBRT) for optimal tumour control with minimum toxicities. The availability of functional imaging modalities such as Magnetic Resonance Imaging (MRI) spectroscopy [1-6], 11C-Choline Positron Emission Tomography (PET) [7] and 18F-Choline PET [8] allowed better localization of Dominant Intraprostatic Lesions (DIL) for possible dose escalation to achieve better tumour control probability.

Several clinical studies [9-12] showed that dose escalation to the prostate improves tumor control. Several treatment planning studies on dose escalation to the prostate and to a dominant DIL were conducted previously. These studies included Intensity Modulated Radiation Therapy (IMRT) and Tomotherapy [13], simultaneous integrated IMRT boost [14] and Volumetric Modulated Arc Therapy (VMAT) [15]. A clinical study on 22 patients using IMRT was performed to assess the feasibility of

escalating the dose to a DIL identified by magnetic resonance imaging (MRI) and magnetic resonance spectroscopy (MRS) [16].

Dose escalation to a very small volume of dominant intraprostatic lesion using IMRT or VMAT may be limited by uncertainties of DIL position during or between radiotherapy sessions. Breathing has little effect on intrafraction prostate motion if the patient is comfortable in the supine position [17, 18]. However, variations in the bladder and rectum filling contribute to inter and intra-fraction prostate motions [19]. These variations can result in prostate motion during EBRT while the patient is on the treatment couch (Intrafractional motion) or between different days of treatment (Interfractional motion). The variations can be accounted for by adding margins to the clinical target volume (CTV) if 3D conformal therapy is used. However, the inter-play effects of IMRT or VMAT [20-22] due to intra-fractional tumour motion can not be accounted for with margin. A study [23] using the Calypso 4D localization system (Calypso System, Calypso Medical, Seattle, WA, USA) provided continuous, real-time localization and monitoring of the prostate. The study reported different prostate motion patterns during the delivery of radiation therapy. While a number of studies have computer simulations investigating the impact of inter- and intra- prostate motion on the dose distributions [24-27], few had measured the delivered dose distributions that incorporated motion uncertainties.

In the present study, we compared a series of treatment plans delivered to a phantom with and without modeled prostate motions. The plans consisted of 76 Gy to the entire prostate with dose escalation to 86 Gy to a hypothetical DIL one eighth the size of the prostate, located in the posterior-inferior-left side of the prostate. The reason for

choosing this DIL location is that many intraprostatic lesions are located near the rectal wall [28]. This comparison included sequential and simultaneous IMRT and VMAT boosts to the DIL. We investigated experimentally the impact of intrafractional prostate motion on the dose distributions of VMAT and IMRT boost plans to a DIL. This provides a more realistic comparison of treatment plans with dose escalation to the DIL including both plan delivery and motion uncertainties.

2.2 Methods and Materials

2.2.1 Treatment planning

A series of six treatment plans were generated for two patients CT scans using Pinnacle^3 treatment planning system (Philips Medical, Andover, Massachusetts, USA) as listed in table 1. The prostate, the gross target volume (GTV), the rectum, the bladder and femoral heads were contoured by a radiation oncologist. Patient 1 (P1) had a larger prostate (72 cc) and rectum (65 cc) but a smaller bladder (110 cc). Patient 2 (P2) had a relatively smaller prostate (59 cc) and rectum (47 cc) but a larger bladder (201 cc). A hypothetical DIL, one eighth the size of the prostate, was contoured in the posterior-inferior-left side of the prostate (DIL_GTV). A 7 mm margin was added in all directions to the prostate GTV to create the prostate planning target volume (prostate_PTV) and to the DIL_GTV to create DIL_PTV to account for random and systematic uncertainties. The six plans generated for each patient were combinations of sequential and simultaneous boost using IMRT and VMAT. A dose of 86 Gy was prescribed to DIL_PTV and 76 Gy to the prostate_PTV in 35 fractions for all the plans. As a reference, IMRT and VMAT plans were also generated with a prescription of 86 Gy to the

prostate_PTV. The IMRT plans consisted of five beams at gantry angles 45°, 105°, 180°, 255°, 315°. The VMAT plans included a single 360° dynamic arc. The IMRT simultaneous boost plan was generated with 18 MV photon energy and the VMAT simultaneous boost plan were generated with 6 MV photon energy and prescribed to be delivered in 35 fractions. All sequential plans were composed of a 5-field IMRT or 360° dynamic ARC plan with 10 Gy boost to the DIL_PTV delivered in either 5 or 35 fractions and a second IMRT or ARC plan with 76 Gy prescribed to the prostate_PTV delivered in 35 fractions. For all the sequential plans, the treatment is delivered in 35 fractions. For the 5 fractions boost plans, the first five fractions will include the delivery of the boost and the prostate_PTV plans and the remaining 30 fractions will consist of the delivery of the prostate_PTV plan only. As for the 35 fractions boost plans, each fraction consists of a boost plan and a prostate_PTV plan delivery. Table 2.1 lists all the plans that were generated and compared.

2.2.2 Plans evaluation and comparison

For a plan to be considered acceptable, at least 95% of the DIL_PTV volume must receive a dose of 86 Gy and at least 95% of the prostate_PTV must receive a dose of 76 Gy. Another criterion is that less than or equal to 2% of the DIL_PTV volume should receive a maximum dose not exceeding 94.6 Gy. The guidelines set by the Radiation therapy Oncology Group (RTOG-0126) listed in Table 2.2 were used for dose volume constraints of rectum and bladder.

	DIL_PTV	Prostate_PTV
Plan 1	5 field IMRT (5 fx)	5 field IMRT (35 fx)
Plan 2	360° Dynamic ARC (5 fx)	360° Dynamic ARC (35 fx)
Plan 3	5 field IMRT (35 fx)	5 field IMRT (35 fx)
Plan 4	360° Dynamic ARC (35 fx)	360° Dynamic ARC (35 fx)
Plan 5	Simultaneous boost 5 field IMRT	
Plan 6	Simultaneous boost 360° Dynamic ARC	

Table 2.1. A list of the generated plans for both patient CT scans.

Organ At Risk	Type	Objective
Rectum	Maximum relative volume exceeding dose 75 Gy, 70 Gy, 65 Gy, and 60 Gy	15%, 25%, 35%, and 50%
Bladder	Maximum relative volume exceeding dose 80 Gy, 75 Gy, 70 Gy, and 65 Gy	15%, 25%, 35%, and 50%

Table 2.2. The rectum and bladder planning guidelines set by the Radiation therapy Oncology Group (RTOG-0126).

Dose Volume Histograms (DVHs), dose distributions, minimum, maximum and mean dose of the DIL_PTV, rectum and bladder were used for plans comparison. Dose uniformity within the DIL_PTV and dose spillage outside the prostate_PTV were also used to evaluate the quality of a plan.

2.2.3 Plan delivery and dose measurements

2.2.3.1 Plan delivery

All plans were delivered on a VARIAN clinical linear accelerator (CLINAC iX) with RapidArc delivery capability (VARIAN Medical Systems, Palo Alto, California, USA). All generated plans were first imported to a record and verify system (ARIA, VARIAN oncology information management software). Delivered dose was measured using MapCHECK™ with MapPHAN™ (Sun Nuclear Corporation, Melbourne, Florida, USA). MapCHECK™ is a diode array that consists of 445 SunPoint Diode detectors distributed over a 20 × 20 cm grid. The detector spacing is 7.07 mm over the inner 10 × 10 cm area and 14.04 mm over the outer 10 × 10 cm area. Absolute dose measured on diodes were compared to planned dose points using Gamma analysis method. MapPHAN™ is a homogeneous water equivalent phantom that holds MapCHECK™ at isocenter for rotational dosimetry. The MapCHECK™-MapPHAN™ system can support measurements in the coronal and sagittal planes. 10 cm buildup was used for MapCHECK™-MapPHAN™ system as shown in Figure 2.1.

All doses were measured using MapCHECK™-MapPHAN™ system set in the sagittal plane. The original plan on the patient CT is copied to the CT of MapCHECK™-MapPHAN™ system and the dose is calculated with the plan isocenter relocated to the center of the MapCHECK™-MapPHAN™ system. A planar dose of the plan is generated on the MapCHECK™-MapPHAN™ system CT to compare with the measurements.

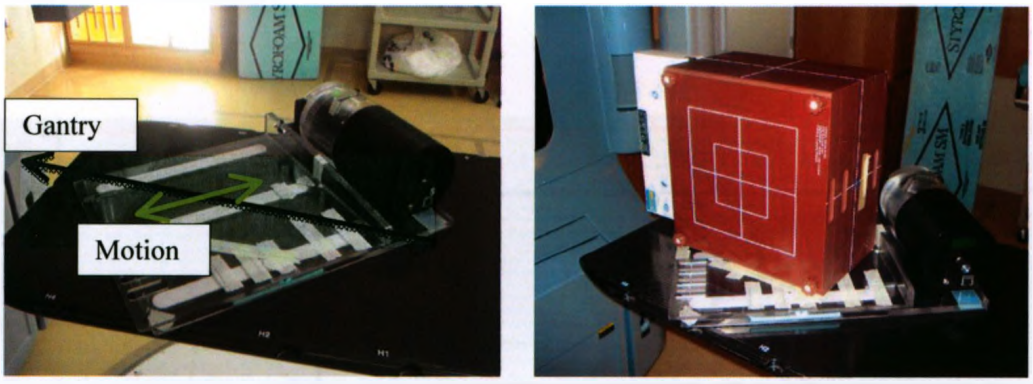

(a) (b)

Figure 2.1. (a) The motion platform rotated by 40° on the treatment couch relative to the sagittal laser in the treatment room, (b) The MapCHECK™-MapPHAN™ system rotated by 90° counterclockwise around the sagittal laser in the sagittal plane and set on the rotated motion platform.

2.2.3.2 Incorporation of prostate motion

A one dimensional programmable motion platform (QUASAR™ Programmable Respiratory Motion Platform, Modus Medical Devices, London, Ontario, Canada) was used for this experiment. The platform has dimensions of 35 × 35 cm and can hold a maximum weight of 20 kg. The platform can be operated manually or be controlled by programmable motion patterns. A clinical study [20] showed that there are 4 typical motion patterns. The study showed that the motion in the longitudinal (superior-inferior) and the vertical (anterior-posterior) directions are more prominent than the motion in the lateral (right-left) direction. It also showed that the longitudinal and vertical motions are correlated in all patterns. These 4 patterns were modeled and programmed into the motion platform software as shown in Figure 2.2. A 2 mm systematic shift in the amplitude of the motion platform was observed when the MapCHECK™-MapPHAN™

system was set on the motion platform. This systematic shift occurred for all patterns and was observed consistently.

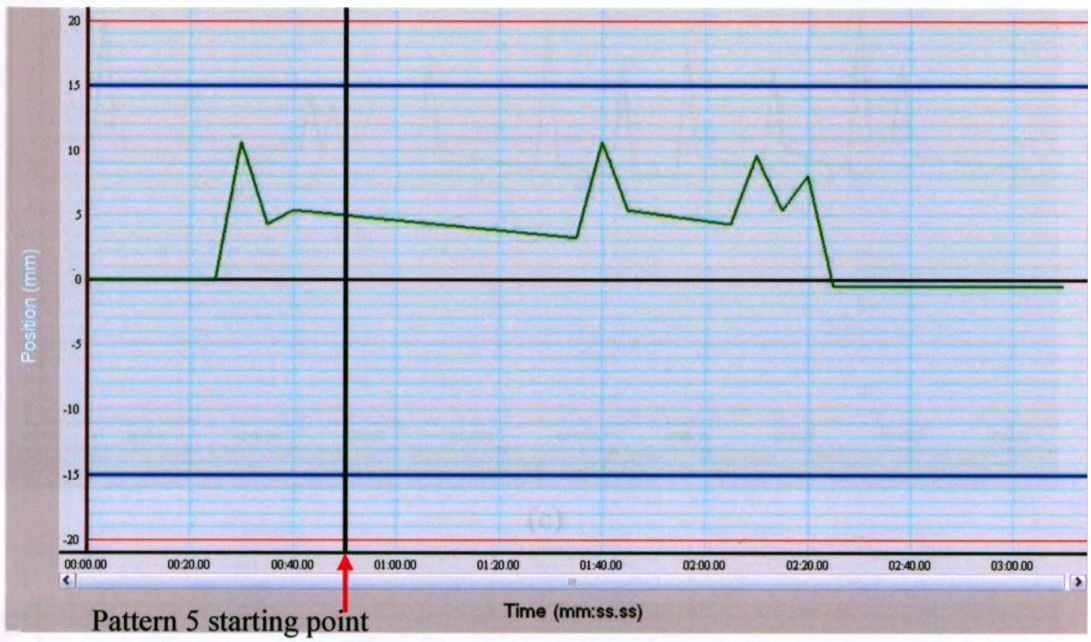

(a)

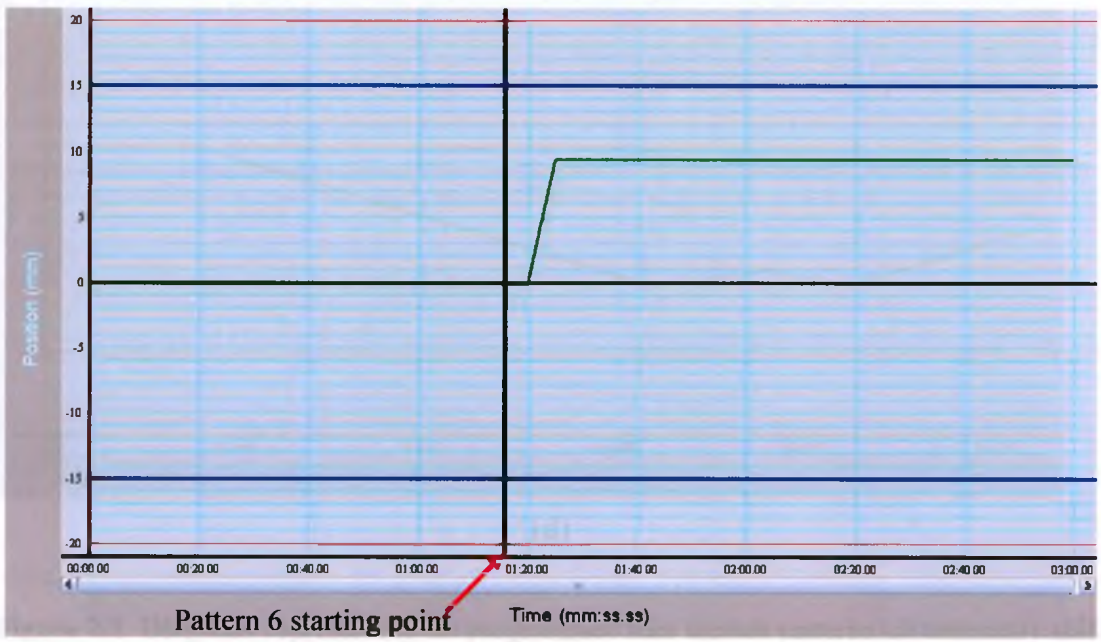

(b)

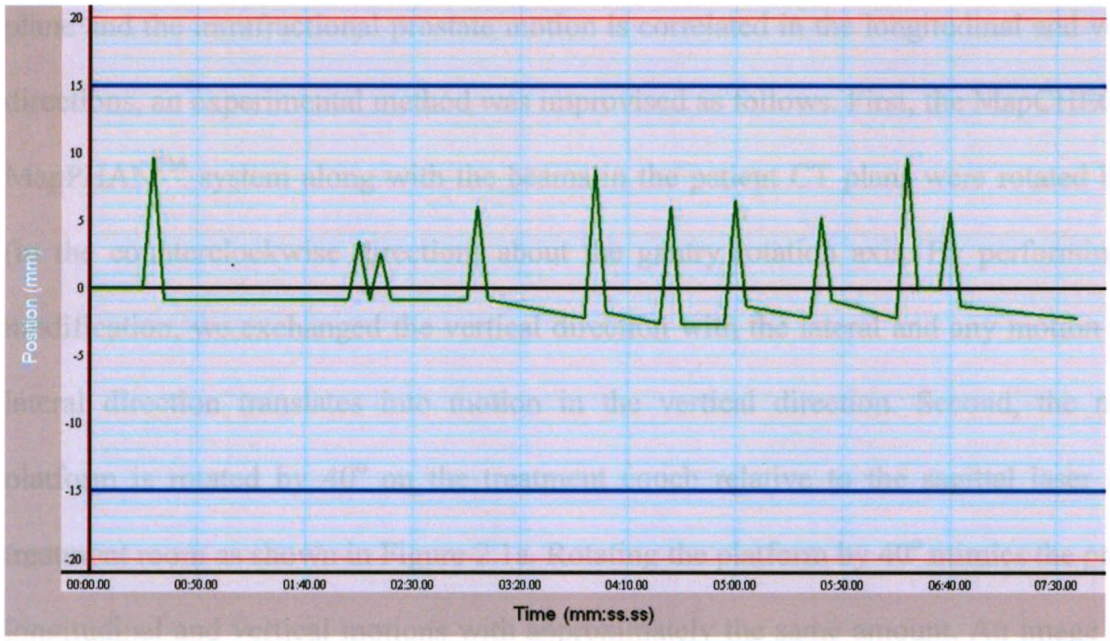

(c)

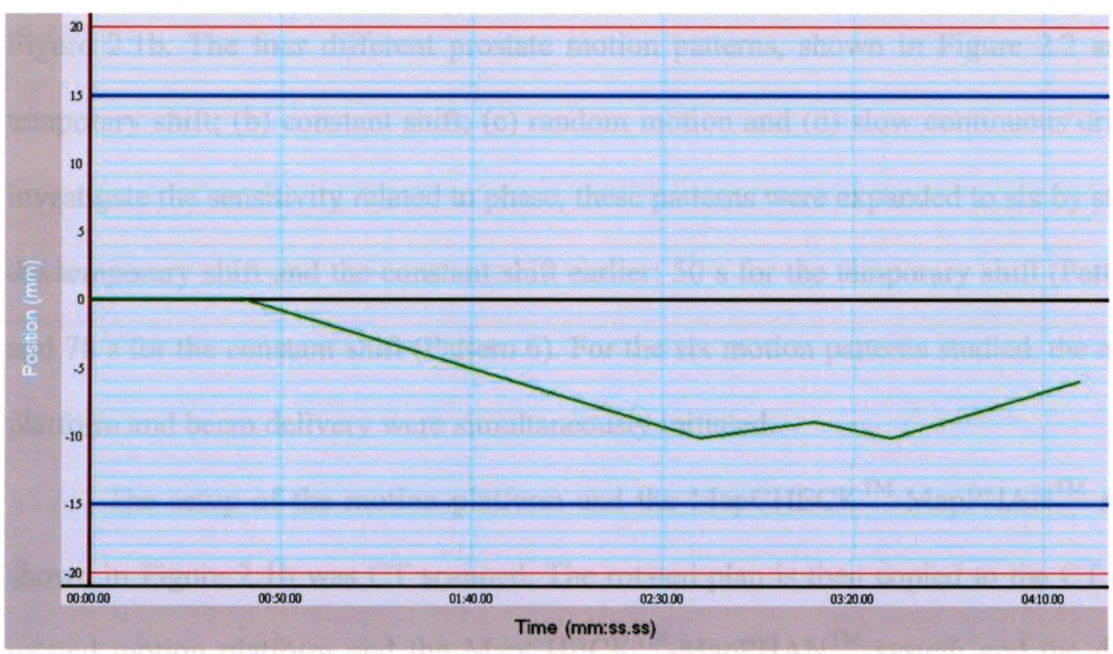

(d)

Figure 2.2. Diagrams representing the programmed four motion patterns (a) temporary shift pattern (SI total extent from 0 to 9 mm – AP total extent from 0 to 7 mm), (b) constant shift pattern (SI total extent from 0 to 8 mm – AP total extent from 0 to 6 mm), (c) random motion pattern (SI total extent from −2 to 7 mm – AP total extent from −2 to 8 mm), and (d) slow continuous drift pattern (SI total extent from 0 to −7 mm – AP total extent from 0 to −7 mm).

Since the motion platform is programmable only in one direction in the coronal plane and the intrafractional prostate motion is correlated in the longitudinal and vertical directions, an experimental method was improvised as follows. First, the MapCHECK™-MapPHAN™ system along with the beams in the patient CT plans were rotated by 90° (in the counterclockwise direction) about the gantry rotation axis. By performing this modification, we exchanged the vertical direction with the lateral and any motion in the lateral direction translates into motion in the vertical direction. Second, the motion platform is rotated by 40° on the treatment couch relative to the sagittal laser in the treatment room as shown in Figure 2.1a. Rotating the platform by 40° mimics the prostate longitudinal and vertical motions with approximately the same amount. An image of the setup of the motion platform and the MapCHECK™-MapPHAN™ system is shown in Figure 2.1b. The four different prostate motion patterns, shown in Figure 2.2 are: (a) temporary shift; (b) constant shift; (c) random motion and (d) slow continuous drift. To investigate the sensitivity related to phase, these patterns were expanded to six by starting the temporary shift and the constant shift earlier: 50 s for the temporary shift (Pattern 5) and 78 s for the constant shift (Pattern 6). For the six motion patterns studied, the motion platform and beam delivery were simultaneously initiated.

The setup of the motion platform and the MapCHECK™-MapPHAN™ system shown in Figure 2.1b was CT scanned. The rotated plan is then copied to the CT of the rotated motion platform and the MapCHECK™-MapPHAN™ system and the dose is calculated. A planar dose is generated on the rotated "motion platform and the MapCHECK™-MapPHAN™ system". Plans were then delivered on the setup shown in Figure 2.1b. Each of the plans in Table 2.1 was delivered seven times: the first with a

stationary system at the neutral position ("no-motion" pattern, Pattern 0) and six times with the platform moving according to the six motion patterns. Dose is recorded with MapCHECK™ for the 7 measurements for each of the 6 plans listed in Table 2.1 for two patients, resulting in 84 2D dose distributions for analyses.

2.2.3.3 Measurement evaluation

Gamma analysis was used to compare the seven measurements with the planar dose for each plan. The Gamma analysis threshold parameters used in this work are 3% percent in dose-difference and 3 mm for distance to agreement. In this particular case, Gamma value will be less than or equal to one if the dose difference is less than or equal to 3% or the distance-to-agreement is less than or equal to 3 mm. Without motion, at least 90% of the compared points must pass the Gamma analysis criteria for a plan to be considered acceptable (i.e at least 90% of the points must have a Gamma value that is less than or equal to 1) [29]. The mean Gamma value was computed and compared for each motion pattern for each investigated plan.

Such Gamma analyses reflect dosimetric accuracies for a 2D plane of each plan. To assess dose delivered specifically to the DIL in the presence of motion, the relative root mean square (*rrms*) of the difference between the delivered dose for all the motion patterns and the delivered "no motion" dose inside a DIL (DIL_GTV) volume is calculated and compared for all the plans for P1. The *rrms* is defined as

$$rrms = \frac{\sqrt{\frac{\sum_i (D_{im} - D_{inm})^2}{N}}}{D_m} \qquad (2)$$

where D_{im} is the measured dose for the ith point inside the DIL_GTV contour for a certain motion pattern, D_{inm} is the measured dose for the corresponding point for the no motion pattern of the same plan, N is the total number of measured dose points inside the DIL_GTV contour and D_m is the average dose inside the DIL_GTV for the no motion pattern. The *rrms* value measures the magnitude of the dose variation inside the DIL_GTV, however these values do not provide information about the fraction of the DIL_GTV receiving the prescribed dose. A method of measuring that is to calculate the percent of measured points receiving at least 90% of the prescribed dose inside the DIL_GTV.

To study the effect of motion for the whole treatment course, planar doses were accumulated according to the probability based on the Calypso data (Calypso System, Calypso Medical, Seattle, WA, USA) [20] in which 59% of the fractions exhibited no motion (Pattern 0), 26% of the fractions assumed motion between 3 – 5 mm (Patterns 1 and 2) and 15% of the fractions assumed motion larger than 5 mm (Patterns 3, 4, 5 and 6). For Plans 1 and 2, two combinations of patterns were used for comparison with three fractions covered by Pattern 0, one fraction by Pattern 1, and the last fraction covered alternatively by Patterns 6 (C5-1) and 3 (C5-2). The reason for choosing these two combinations is to cover the two extreme motion patterns. For the remaining four plans, four combinations of patterns were used to study the motion effect on the total treatment course: C35-1 to C35-4 as listed in Table 2.3. In addition to these combinations, an average combination was considered. In this combination, the mean Gamma value for each pattern was weighted according to its probability and an average Gamma value for the whole treatment course was obtained.

Combination	Patterns
C35-1	(a) 21 fractions Pattern 0 (b) 9 fractions Pattern 1 (c) 5 fractions Pattern 6
C35-2	(a) 21 fractions Pattern 0 (b) 9 fractions Pattern 1 (c) 5 fractions Pattern 3
C35-3	(a) 21 fractions Pattern 0 (b) 5 fractions Pattern 1 (c) 4 fractions Pattern 2 (d) 3 fractions Pattern 3 (e) 1 fraction Pattern 4 (f) 1 fraction Pattern 5
C35-4	(a) 21 fractions Pattern 0 (b) 5 fractions Pattern 1 (c) 4 fractions Pattern 2 (d) 2 fractions Pattern 3 (e) 1 fraction Pattern 4 (f) 1 fraction Pattern 5 (g) 1 fraction Pattern 6

Table 2.3. The probability weighted combinations for the 35 fractions plans along with patterns used for each combination.

2.3 Results

2.3.1 Plan comparison

Figure 2.3 displays the dose distribution and the DVHs of Prostate_PTV, rectum and bladder for the whole prostate dose escalation plans (IMRT and VMAT) for P1. In both plans the rectum and the bladder exceeded the RTOG 0126 guidelines. For example, more than 15% of the bladder volume exceeded 87 Gy for the IMRT plan and 88 Gy for the ARC plan respectively. Similarly, doses to 25% and 35% of bladder volumes were exceeded for both plans. As for the rectum more than 15% of its volume exceeded 80 Gy and 79 Gy for the IMRT plan and the ARC plan respectively. Similar results were obtained for P2.

Figure 2.4 shows the dose distribution and the DVHs (prostate_PTV, DIL_PTV, rectum and bladder) for the simultaneous IMRT and VMAT plans with 76 Gy to whole prostate and 10 Gy boost to DIL. Both plans met the constraints on the rectum and bladder while satisfying the prostate_PTV and DIL_PTV prescription objective. The dose distribution and the DVHs (prostate_PTV, DIL_PTV, rectum and bladder) for two sequential plans (Plan 1 and Plan 2 from Table 1) are shown in Figure 2.5. Table 2.4 lists the minimum, maximum and mean dose values for the DIL_PTV and the Prostate_PTV – DIL_PTV. Similar results were observed for Plans 3 and 4 for P1 and similar results were found for P2 for all plans. All plans passed the criteria set for plan evaluation.

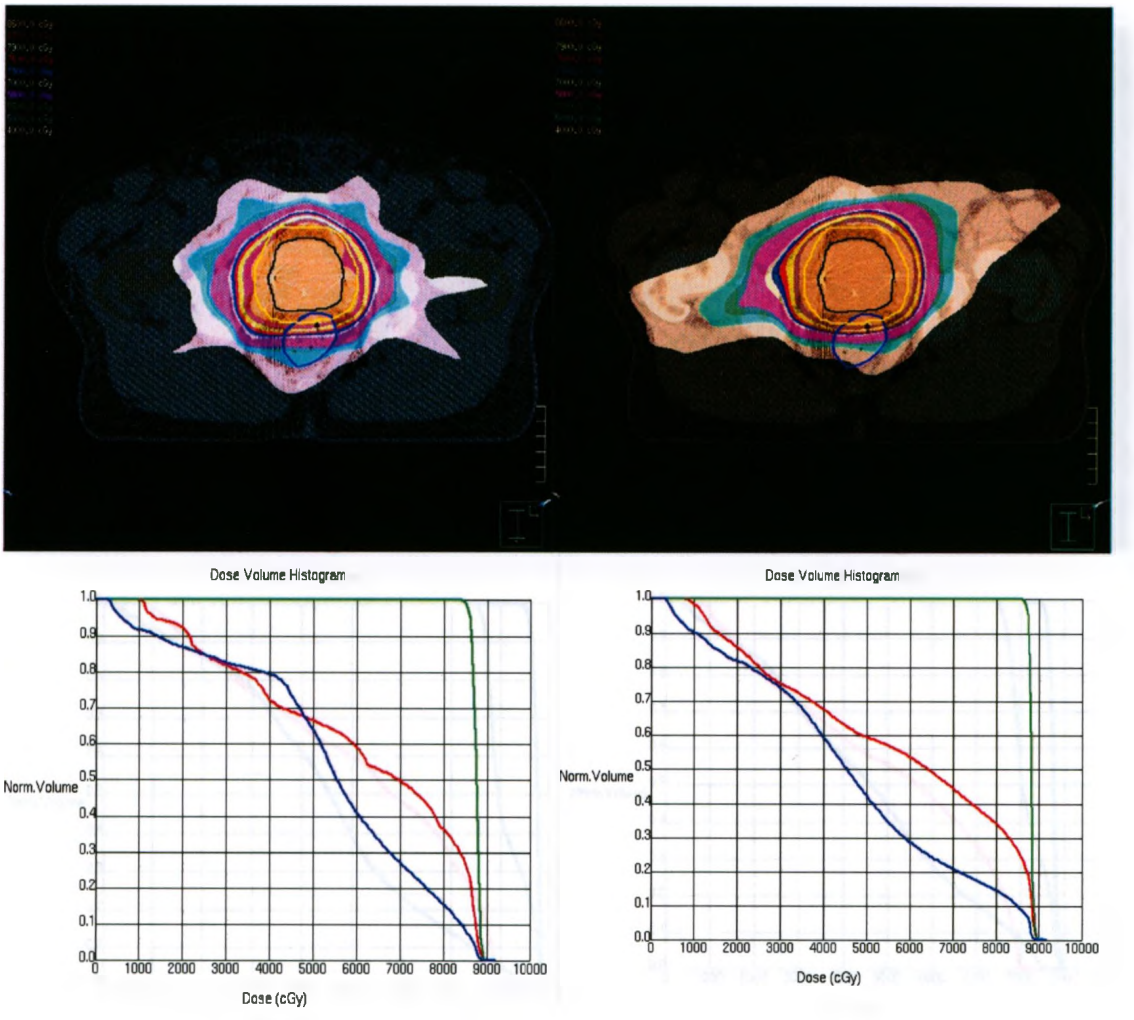

(a) IMRT (b) VMAT

Figure 2.3. A transverse slice dose distribution and DVHs for the rectum (blue), bladder (red) and the prostate_PTV (green) for the whole prostate dose escalation to 86 Gy for P1. (a) IMRT Plan, (b) VMAT plan.

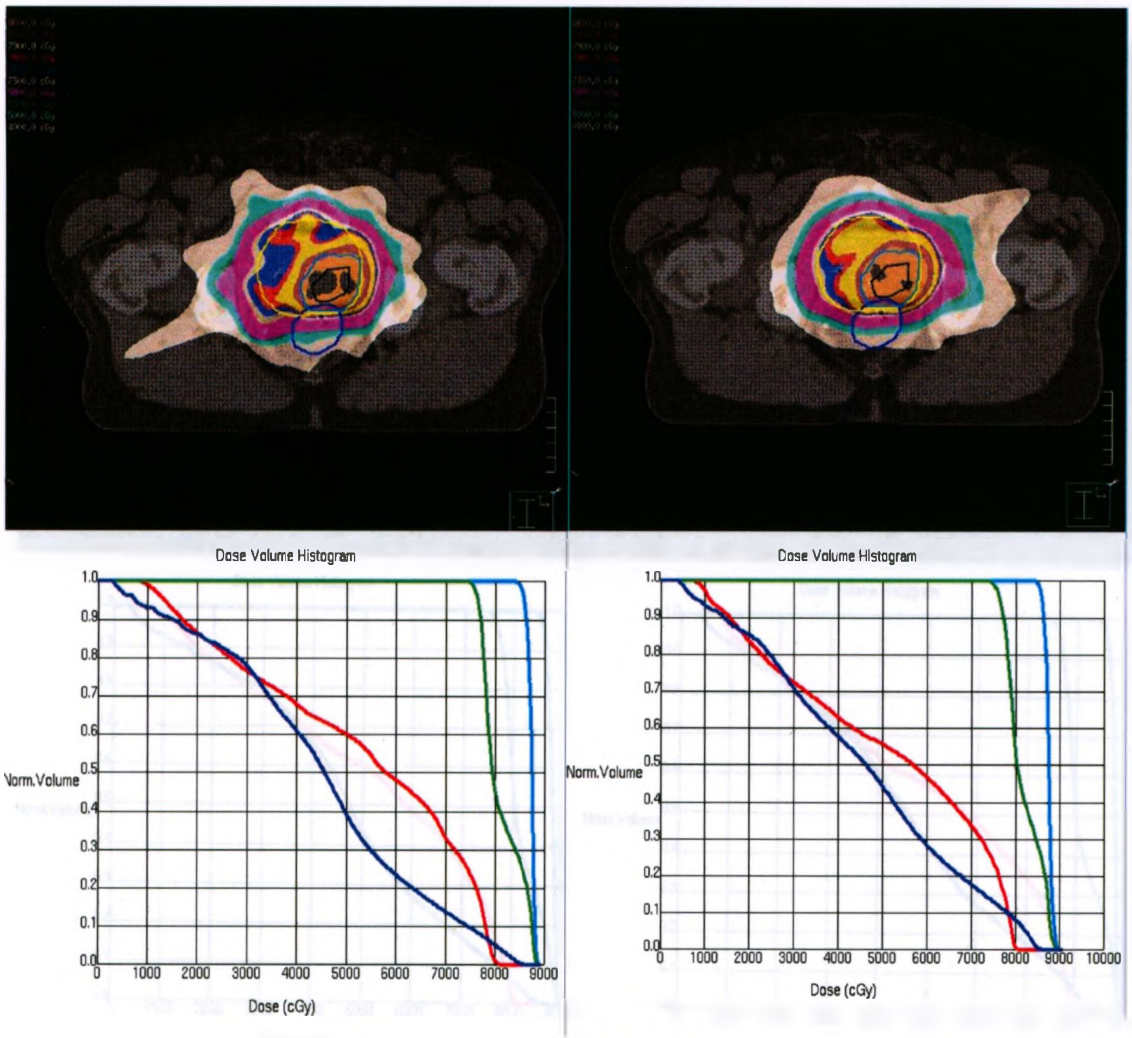

(a) Simultaneous IMRT (b) Simultaneous VMAT

Figure **2.4**. A transverse slice dose distribution and DVHs for the rectum (blue), bladder (red) and the prostate_PTV (green) and the DIL_PTV (light blue) for the simultaneous DIL boost plans for P1. (a) IMRT Plan, (b) VMAT plan.

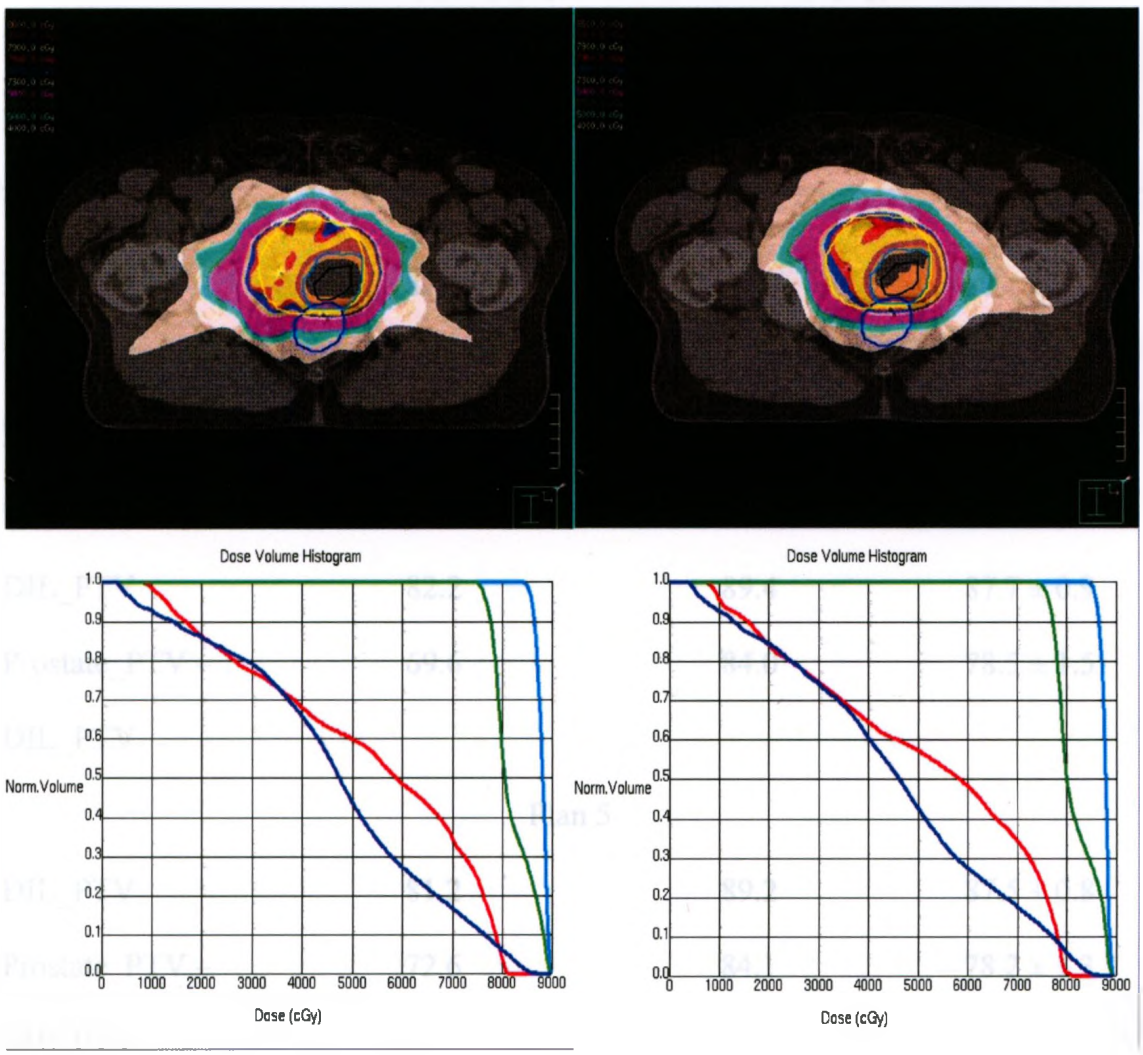

(a) Plan 1 (b) Plan 2

Figure 2.5. A transverse slice dose distribution and DVHs for the rectum (blue), bladder (red) and the prostate_PTV (green) and the DIL_PTV (light blue) for the sequential DIL_PTV boost plans for P1 (high total MU/fx). (a) IMRT Plan (Plan 1), (b) VMAT plan (Plan 2).

	Minimum Dose (Gy)	Maximum Dose (Gy)	Mean Dose ± Standard Deviation (Gy)
		Plan 1	
DIL_PTV	82.3	89.9	88.1 ± 1.1
Prostate_PTV – DIL_PTV	72.6	83.4	79.0 ± 0.5
		Plan 2	
DIL_PTV	82.2	89.4	87.7 ± 0.9
Prostate_PTV – DIL_PTV	69.6	84.0	78.5 ± 1.5
		Plan 5	
DIL_PTV	81.2	89.2	87.5 ± 0.8
Prostate_PTV – DIL_PTV	72.6	84.1	78.2 ± 1.3
		Plan 6	
DIL_PTV	83.6	90.1	87.6 ± 0.9
Prostate_PTV – DIL_PTV	71.2	84.1	78.8 ± 1.6

Table 2.4. The minimum, maximum, and mean dose values for the DIL_PTV and the Prostate_PTV – DIL_PTV for Plans 1, 2, 5 and 6 (from Table 2.1).

2.3.2 IMRT and VMAT dose delivery with prostate motion

Figure 2.6 shows a comparison between measured dose and planned dose from a single fraction of the IMRT and VMAT simultaneous plans for different motion patterns, including the no-motion pattern. The no-motion pattern reported Gamma analysis for the two plans, with pass rate 96.2% for the IMRT plan and 98.4% for the VMAT plan. Table 2.5 lists the mean Gamma values for the six motion patterns for all investigated plans for P1 and P2. All plans demonstrated the least sensitivity to motion Pattern 3 with the lowest mean Gamma values while the highest sensitivity is to motion Pattern 6. Pattern 6 mean Gamma values exceeded 1.0 for most of the plans presented. This could be explained by comparing motion patterns 3 and 6. Motion Pattern 3 represents a random motion pattern in which the motion changes directions continuously in a random manner, in a sense that the total motion effect averages out. Whereas motion Pattern 6 represents the extreme case for prostate motion, a large shift (10 mm total displacement) that starts few seconds after the start of the treatment and clearly it should have the highest motion sensitivity. While individual Gamma values for the different motion patterns varied, the overall mean Gamma value of the VMAT simultaneous plan is less than the IMRT simultaneous plan for both patients. This overall behavior could be explained by considering the total MU for both plans. In general, the simultaneous IMRT plan has larger total MU than the VMAT simultaneous plan, thus resulting in longer delivery times which will make the IMRT simultaneous plan more susceptible to motion than the VMAT simultaneous plan. On the other hand, the overall maen Gamma value for IMRT boost-only 5 fractions (high MU/fraction(fx)) plans are lower than VMAT boost-only plans. The effect of motion for IMRT plans depends only on motion during delivery. For

certain patterns, abrupt motion might occur when the beam is off and the motion will not affect the delivery in that case, whereas for VMAT plans the beam is being delivered continuously and any motion occurred during delivery it will affect the final outcome. Another factor that can influence the sensitivity to motion for the IMRT plans is the user dependency. The sensitivity to intrafractional motion depends on the instances at which the user starts each beam during delivery. This was not a concern for the VMAT plans since the beam is initiated only once during delivery.

The extreme motion that is represented by Pattern 6 will create a large distance to agreement, which in turn led to a high mean Gamma value.

In Figure 2.7 the measured dose and the planned dose for the VMAT DIL_PTV boost in 35 fractions (total MU/fx = 134) and VMAT DIL_PTV boost in 5 fractions (total MU/fx = 488) are compared for motion Patterns 1, 2, 3 and 4. The mean Gamma values in Table 2.5 demonstrated lower trend for the high total MU/fx VMAT DIL_PTV boost plans than the low total MU/fx VMAT DIL_PTV boost plans. This can be attributed to the fact that delivering the low total MU/fx results in too low MU per control point. Delivering a too low MU per control point has higher delivery uncertainty than the high MU per control (high total MU/fx) VMAT. [30] This became an additional source of uncertainty during delivery.

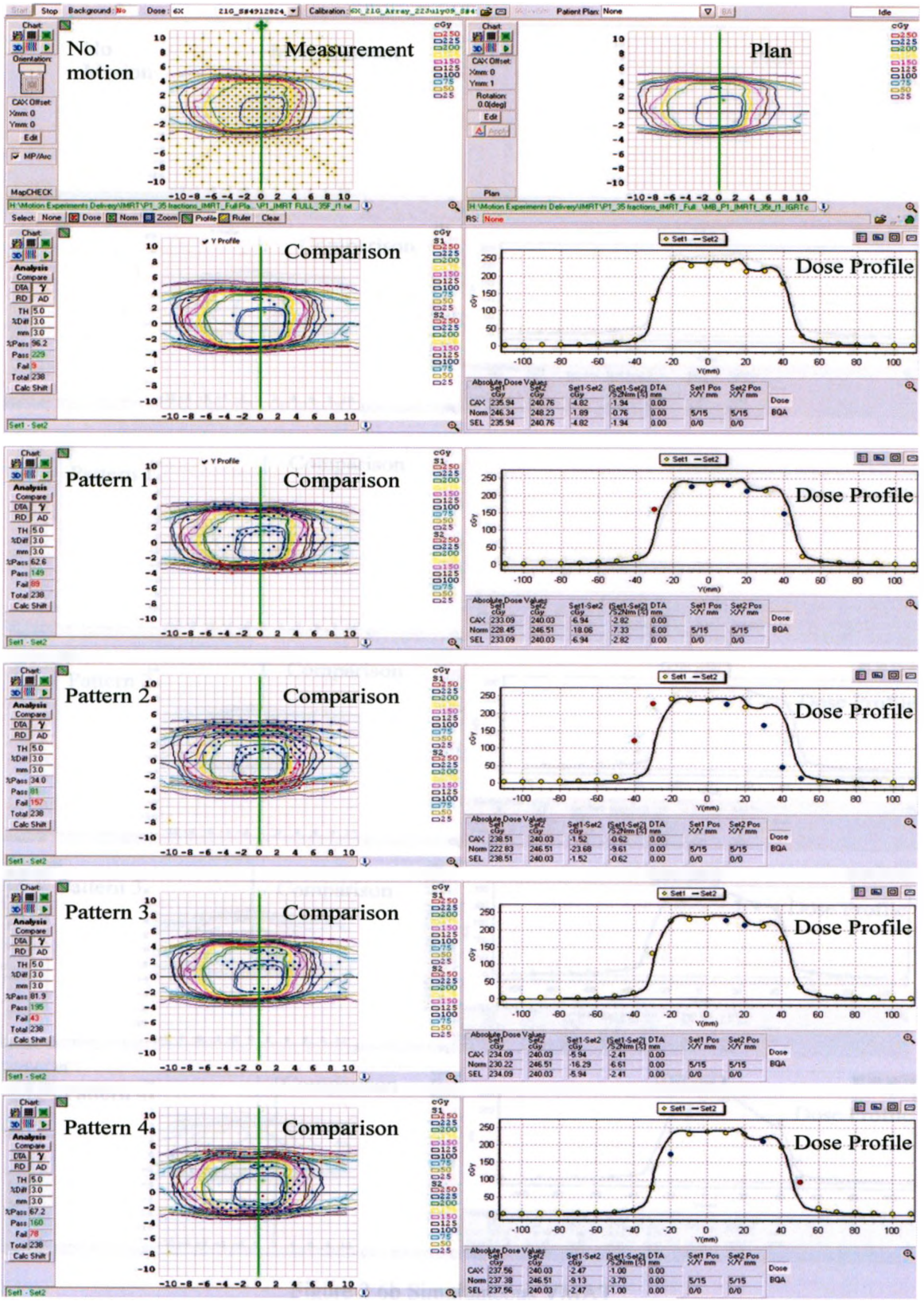

Figure 2.6a Simultaneous IMRT

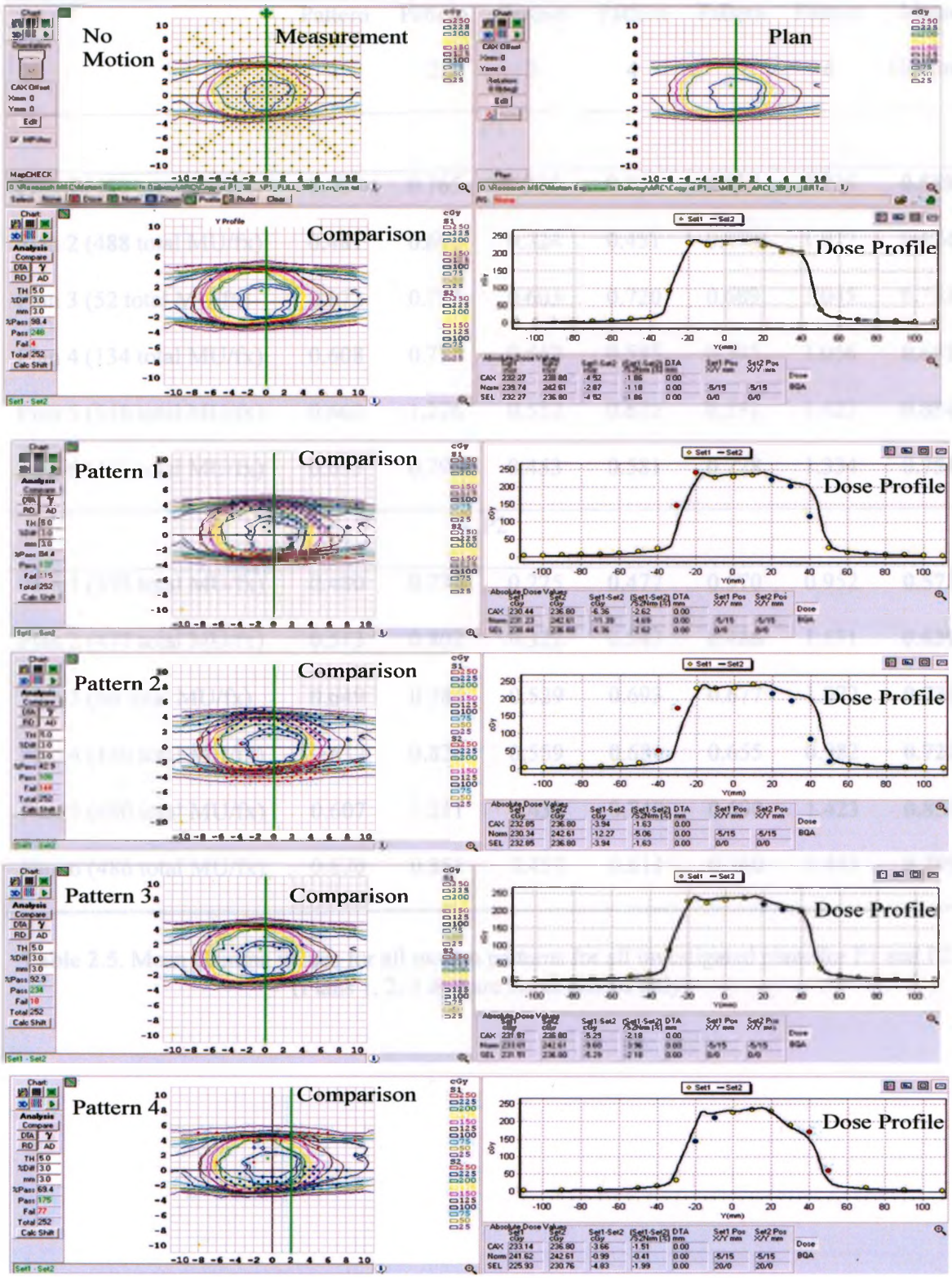

Figure 2.6b Simultaneous VMAT

Figure 2.6. Measurement and calculated planar dose comparison for the no-motion pattern, Pattern 1, Pattern 2, Pattern 3 and Pattern 4 for P1. (a) IMRT simultaneous DIL_PTV boost plan, (b) VMAT simultaneous DIL_PTV boost plans.

	Pattern 1	Pattern 2	Pattern 3	Pattern 4	Pattern 5	Pattern 6	Mean Gamma
			P1				
Plan 1 (460 total MU/fx)	0.429	0.765	0.236	0.455	0.530	0.936	**0.558**
Plan 2 (488 total MU/fx)	0.481	0.698	0.324	0.451	0.470	1.022	**0.574**
Plan 3 (52 total MU/fx)	0.672	0.731	0.603	0.720	0.689	1.045	**0.743**
Plan 4 (134 total MU/fx)	0.608	0.782	0.452	0.595	0.595	1.056	**0.681**
Plan 5 (548 total MU/fx)	0.662	1.226	0.552	0.672	0.591	1.423	**0.854**
Plan 6 (493 total MU/fx)	0.633	0.796	0.453	0.581	0.728	1.334	**0.754**
			P2				
Plan 1 (395 total MU/fx)	0.480	0.734	0.225	0.477	0.570	0.952	**0.573**
Plan 2 (477 total MU/fx)	0.513	0.802	0.322	0.543	0.486	1.171	**0.639**
Plan 3 (66 total MU/fx)	0.649	0.784	0.529	0.693	0.677	1.072	**0.734**
Plan 4 (140 total MU/fx)	0.632	0.826	0.559	0.681	0.655	0.982	**0.722**
Plan 5 (480 total MU/fx)	0.607	1.211	0.439	0.740	0.690	1.423	**0.852**
Plan 6 (486 total MU/fx)	0.670	0.851	0.459	0.613	0.760	1.443	**0.799**

Table 2.5. Mean Gamma values for all motion patterns for all investigated plans for P1 and P2. (Plans 1, 2, 3 & 4 are boost phases only)

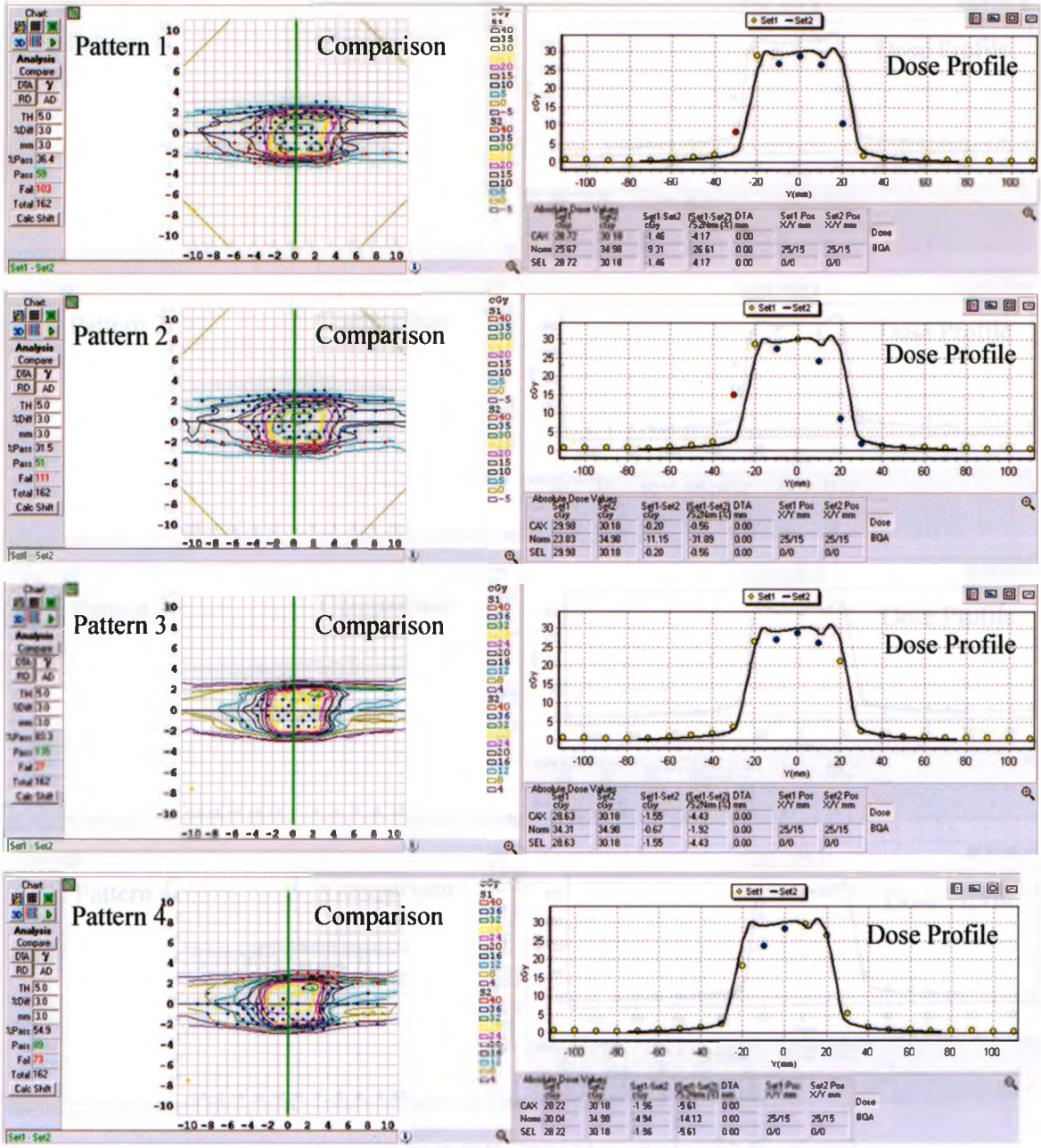

Figure 2.7a VMAT DIL_PTV boost plan (35 fractions)

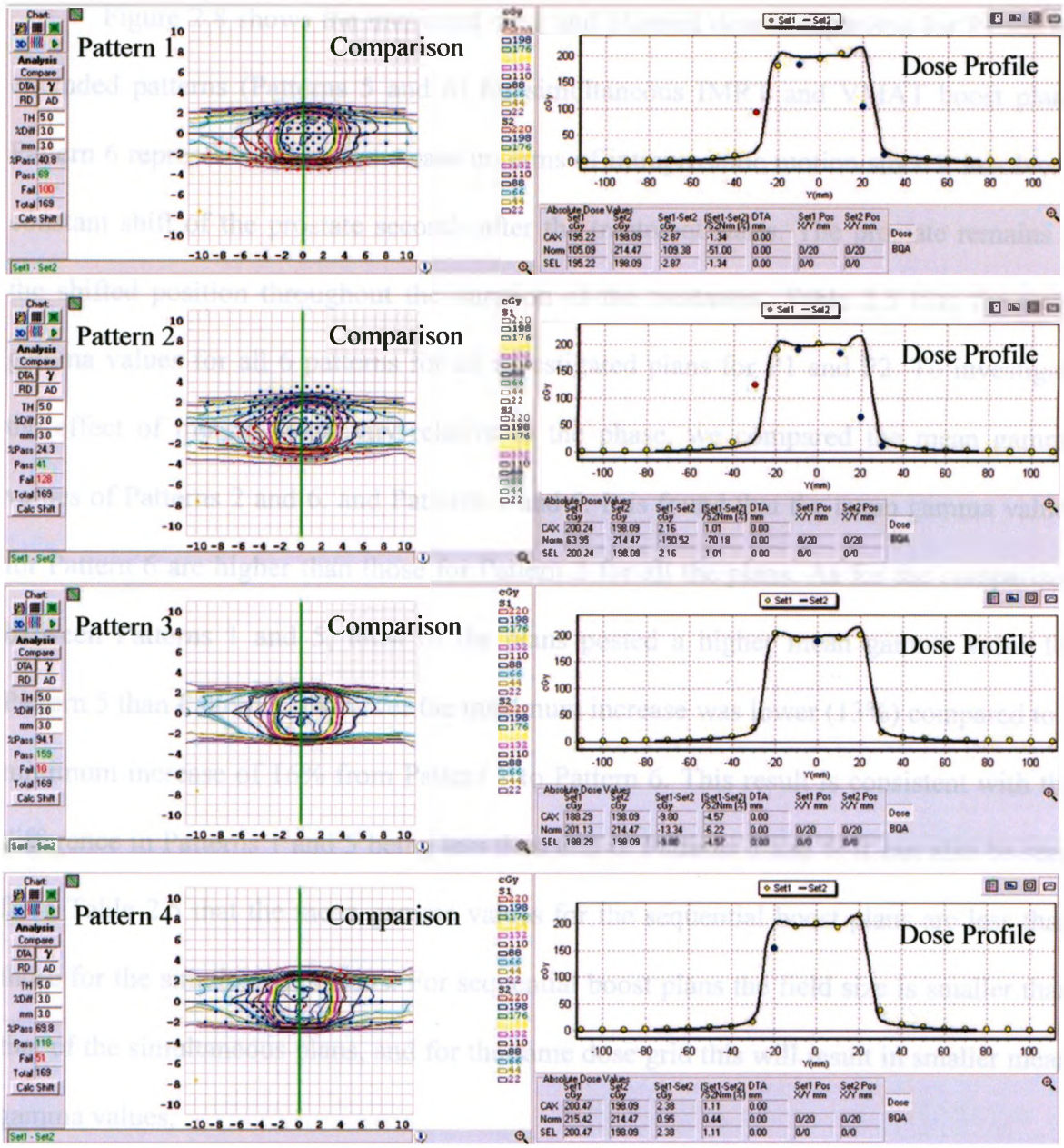

Figure 2.7b VMAT DIL_PTV boost plan (5 fractions)

Figure 2.7. Measurement and calculated planar dose comparison for Pattern 1, Pattern 2, Pattern 3 and Pattern 4 for P1. (a) 134 total MU/fx VMAT DIL_PTV boost plan, (b) 488 total MU/fx VMAT DIL_PTV boost plan.

Figure 2.8 shows the measured dose and planned dose comparison for P1 for the extended patterns (Patterns 5 and 6) for simultaneous IMRT and VMAT boost plans. Pattern 6 represents the extreme case in terms of intraprostatic motion since it involves a constant shift of the prostate seconds after the treatment starts. The prostate remains at the shifted position throughout the duration of the treatment. Table 2.5 lists the mean gamma values for all 6 patterns for all investigated plans for P1 and P2. To investigate the effect of motion sensitivity relative to the phase, we compared the mean gamma values of Patterns 2 and 6, and Patterns 1 and 5. It is found that the mean gamma values for Pattern 6 are higher than those for Pattern 2 for all the plans. As for the comparison between Patterns 1 and 5, most of the plans posted a higher mean gamma value for Pattern 5 than Pattern 1. However the maximum increase was lower (13%) compared to a minimum increase of 16% from Pattern 1 to Pattern 6. This result is consistent with the difference in Patterns 1 and 5 being less than that of Patterns 2 and 6. It can also be seen from Table 2.5 that the mean gamma values for the sequential boost plans are less than those for the simultaneous plans. For sequential boost plans the field size is smaller than that of the simultaneous plans, and for the same dose grid this will result in smaller mean gamma values.

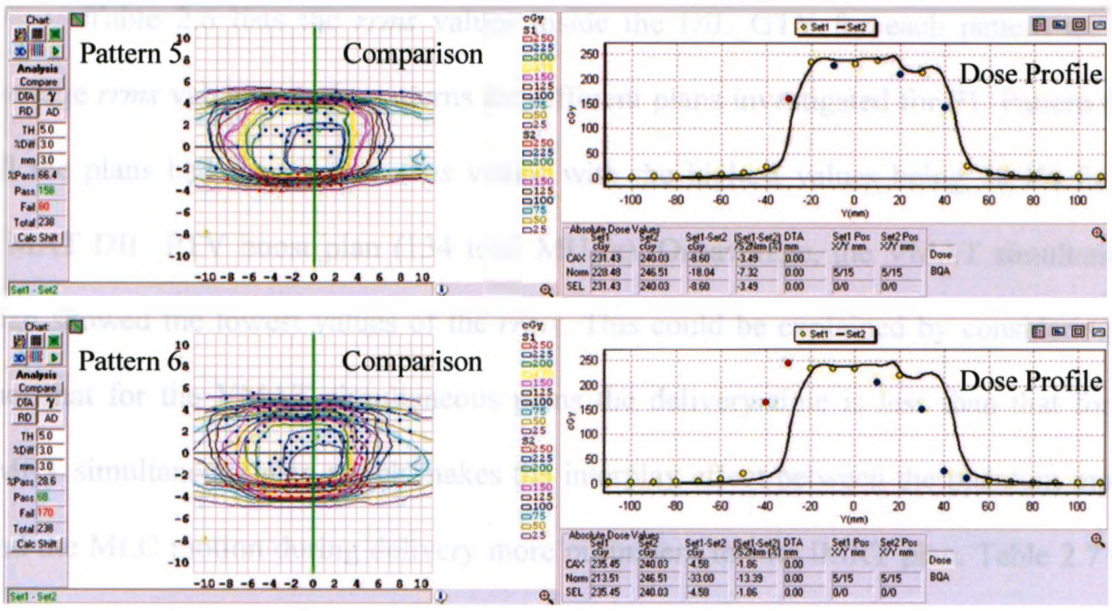

(a) Simultaneous IMRT

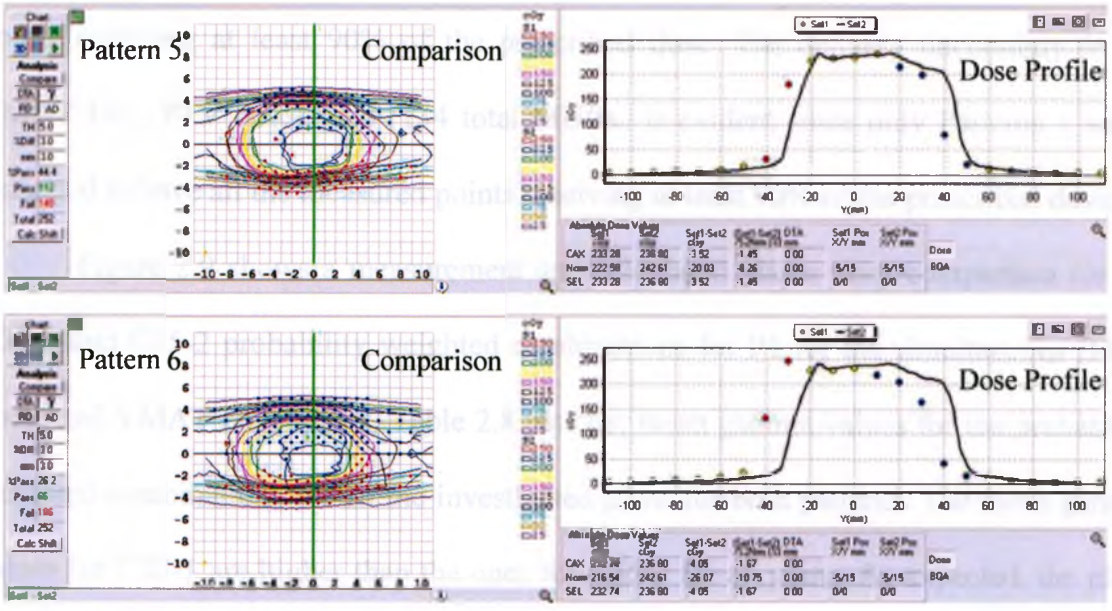

(b) Simultaneous VMAT

Figure 2.8. Measurement and calculated planar dose comparison for Pattern 5, and Pattern 6 for P1. (a) IMRT simultaneous DIL_PTV boost plan, (b) VMAT simultaneous DIL_PTV boost plan.

Table 2.6 lists the *rrms* values inside the DIL_GTV for each pattern and the average *rrms* value over six patterns for different plans investigated for P1. Pattern 6 for all the plans had the highest *rrms* values with the highest values being 18.4% for the VMAT DIL_PTV boost plan (134 total MU/fx). On average, the VMAT simultaneous plan showed the lowest values of the *rrms*. This could be explained by considering the fact that for the VMAT simultaneous plans the delivery time is less than that for the IMRT simultaneous plan which makes the interplay effect between the phantom motion and the MLC motion during delivery more prominent for the IMRT plan. Table 2.7 lists the percent of measured points receiving at least 90% of the prescribed dose inside the DIL_GTV. For the simultaneous plans, all but motion Pattern 6 had all the measured points receiving at least 90% of the prescribed dose. The delivery uncertainty in the VMAT DIL_PTV boost plan (134 total MU/fx) is evident since only Patterns 1 and 4 managed to have all the measured points receiving at least 90% of the prescribed dose.

Figure 2.9 shows a measurement and calculated planar dose comparison for the C35-1 and C35-2 probability weighted combinations for P1 for the simultaneous IMRT boost and VMAT boost plans. Table 2.8 lists the mean gamma values for the probability weighted combinations for all the investigated plans for both patients. The mean gamma values for C35-1 are higher than the ones for C35-2 for all plans. As expected, the plans have less delivery errors when most of the fractions with motion are dominated by the random motion pattern. The VMAT DIL_PTV high total MU/fx boost plan is less sensitive to motion than the low total MU/fx plan for both patients. This result for the 35 fraction simulations are consistent with the results obtained from the single fraction comparisons presented in Table 2.5 and Figure 2.7. It is also expected for the average

values (C5-average and C35-average) to fall between the two extreme combinations. The only exception was for Plan 5 for both patients. The reason for that is the inclusion of Pattern 2 in the average combination and not in the extreme combinations. The average gamma value for Pattern 2 for this particular plan is high and that will increase its weight when it is included in the average value for the whole combination.

	Pattern 1	Pattern 2	Pattern 3	Pattern 4	Pattern 5	Pattern 6	Ave. *rrms*
Plan 1 (460 total MU/fx)	3.1%	6.4%	2.2%	6.6%	5.0%	11.5%	**5.8%**
Plan 2 (488 total MU/fx)	2.9%	3.9%	2.0%	2.4%	4.4%	12.4%	**4.7%**
Plan 3 (52 total MU/fx)	3.8%	4.9%	2.5%	5.0%	2.2%	8.8%	**4.5%**
Plan 4 (134 total MU/fx)	4.5%	5.8%	1.3%	7.4%	6.1%	18.4%	**7.2%**
Plan 5 (548 total MU/fx)	1.4%	1.9%	1.6%	1.9%	1.4%	4.7%	**2.1%**
Plan 6 (493 total MU/fx)	1.4%	1.3%	0.4%	1.6%	1.5%	3.6%	**1.6%**

Table 2.6. The percent *rrms* values inside DIL_GTV and the average *rrms* value for the different motion patterns for the different plans investigated for P1.

	Pattern 1	Pattern 2	Pattern 3	Pattern 4	Pattern 5	Pattern 6	Ave. percent
Plan 1 (460 total MU/fx)	100%	92.3%	76.9%	100%	100%	69.2%	**89.7%**
Plan 2 (488 total MU/fx)	100%	84.6%	100%	100%	100%	76.9%	**93.6%**
Plan 3 (52 total MU/fx)	100%	100%	100%	100%	100%	84.6%	**97.4%**
Plan 4 (134 total MU/fx)	100%	76.9%	92.3%	100%	92.3%	76.9%	**89.7%**
Plan 5 (548 total MU/fx)	100%	100%	100%	100%	100%	76.9%	**96.2%**
Plan 6 (493 total MU/fx)	100%	100%	100%	100%	100%	76.9%	**96.2%**

Table 2.7. The percent of measured points receiving at least 90% of the prescribed dose inside the DIL_GTV for P1.

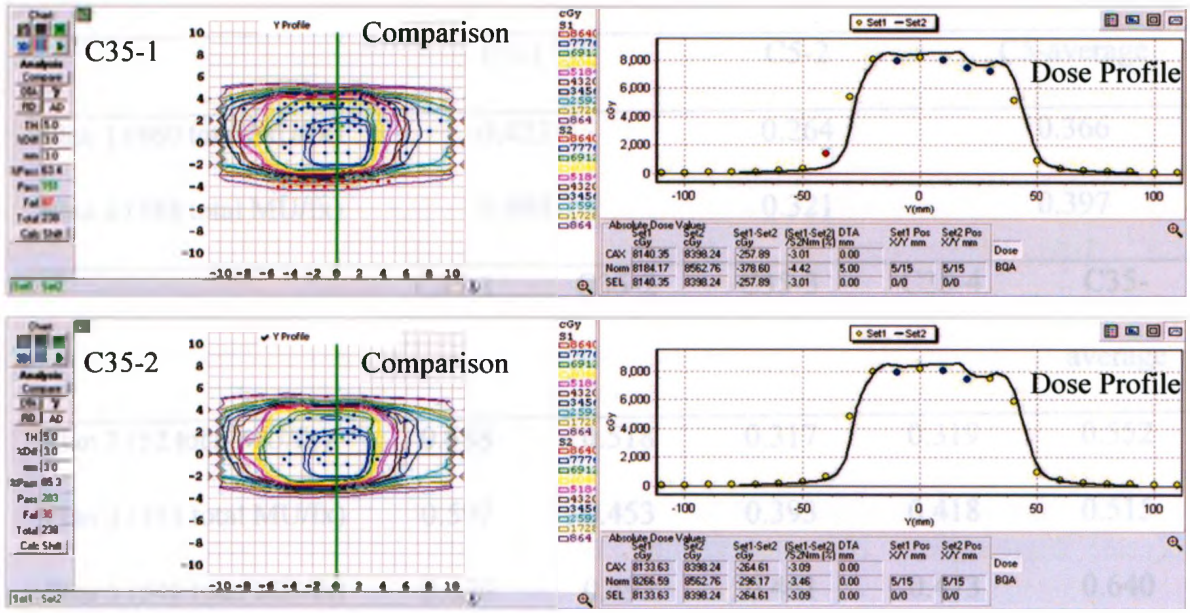

(a) Simultaneous IMRT

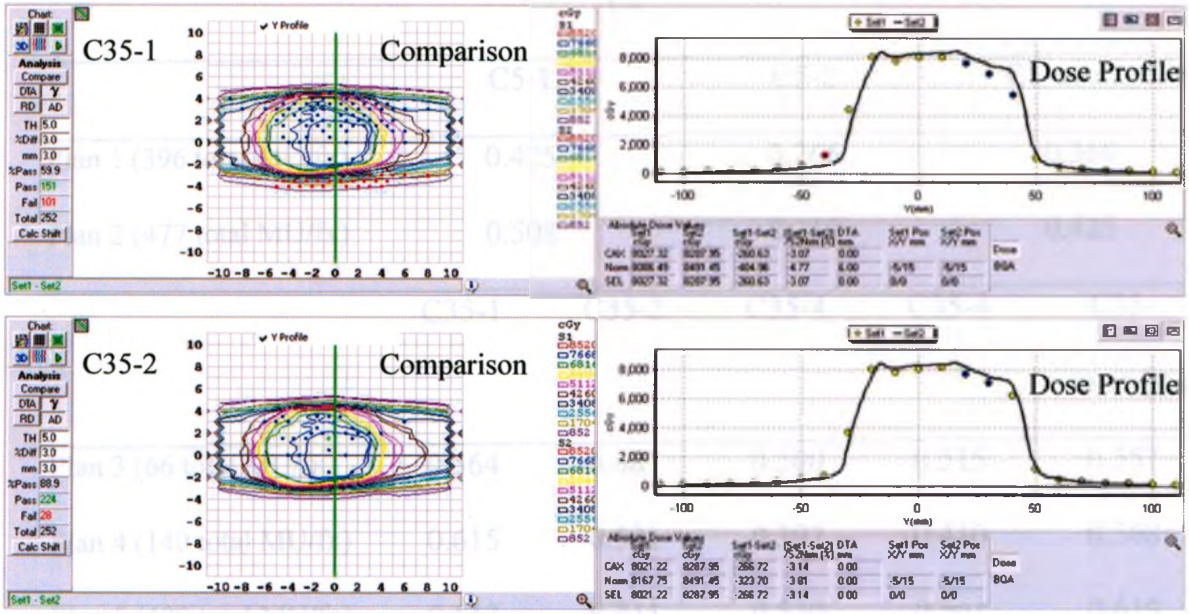

(b) Simultaneous VMAT

Figure 2.9. Measurement and calculated planar dose comparison for the different probability weighted combinations for P1. (a) IMRT simultaneous DIL_PTV boost plan, (b) VMAT simultaneous DIL_PTV boost plan.

P1					
	C5-1		C5-2		C5-average
Plan 1 (460 total MU/fx)	0.423		0.264		0.366
Plan 2 (488 total MU/fx)	0.494		0.321		0.397
	C35-1	C35-2	C35-3	C35-4	C35-average
Plan 3 (52 total MU/fx)	0.588	0.518	0.317	0.319	0.552
Plan 4 (134 total MU/fx)	0.597	0.453	0.393	0.418	0.515
Plan 5 (548 total MU/fx)	0.630	0.493	0.451	0.473	0.640
Plan 6 (493 total MU/fx)	0.609	0.470	0.402	0.416	0.547
P2					
	C5-1		C5-2		C5-average
Plan 1 (396 total MU/fx)	0.425		0.266		0.366
Plan 2 (477 total MU/fx)	0.508		0.312		0.425
	C35-1	C35-2	C35-4	C35-4	C35-average
Plan 3 (66 total MU/fx)	0.564	0.487	0.500	0.515	0.557
Plan 4 (140 total MU/fx)	0.615	0.521	0.397	0.410	0.568
Plan 5 (480 total MU/fx)	0.513	0.411	0.530	0.561	0.619
Plan 6 (486 total MU/fx)	0.621	0.477	0.501	0.531	0.563

Table 2.8. Mean Gamma values for different probability weighted treatment courses for all investigated plans for P1 and P2.

2.4 References

1. Groenendaal G, van den Berg CA, Korporaal JG, *et al.* Simultaneous MRI diffusion and perfusion imaging for tumor delineation in prostate cancer patients. *Radiotherapy and Oncology* 2010;95:185–190.

2. Scheidler J, Hricak H, Vigneron DB, *et al.* Prostate cancer: localization with three-dimensional proton MR spectroscopic imaging – clinicopathologic study. *RAD* 1999;213:473–80.

3. Van Dorsten FA, van der Graaf M, Engelbrecht MRW, *et al.* Combined quantitative dynamic contrast-enhanced MR imaging an 1H NMR spectroscopic imaging of human prostate cancer. *J Magn Reson Imaging* 2004;20:279–87.

4. Fütterer JJ, Heijmink SWTPJ, Scheenen TWJ, *et al.* Prostate cancer localization with dynamic contrast-enhanced MR imaging and proton MR spectroscopic imaging. *Radiology* 2006;241:449–58.

5. Hosseinzadeh K, Schwarz SD. Endorectal diffusion-weighted imaging in prostate cancer to differentiate malignant and benign peripheral zone tissue. *J Magn Reson Imaging* 2004;20:654–61.

6. Miao H, Fukatsu H, Ishigaki T. Prostate cancer detection with 3-T MRI: comparison of diffusion-weighted and T2-weighted imaging. *Eur J Radiol* 2007;61:297–302.

7. Park H, Meyer CR, Wood D, Khan A, *et al.* Validation of Automatic Target Volume Definition as Demonstrated for (11)C-Choline PET/CT of Human Prostate Cancer Using Multi Modality Fusion Techniques. *Acad Radiol.* 2010 May;17(5):614–23.

8. Pinkawa M, Attieh C, Piroth MD, *et al.* Dose-escalation using intensity-modulated radiotherapy for prostate cancer – Evaluation of the dose distribution with and without 18F-choline PET-CT detected simultaneous integrated boost. *Radiotherapy and Oncology* 2009;93(2):213-9.

9. Pollack A, Zagars GK, Starkschall G, *et al.* Prostate cancer radiation dose response: results of the M. D. Anderson phase III randomized trial. *Int J Radiat Oncol Biol Phys* 2002;53(5):1097–1105.

10. Zietman AL, DeSilvio ML, Slater JD, *et al.* Comparison of conventional-dose vs highdose conformal radiation therapy in clinically localized adenocarcinoma of the prostate: a randomized controlled trial. *Jama* 2005;294(10):1233–1239.

11. Dearnaley DP, Hall E, Lawrence D, *et al.* Phase III pilot study of dose escalation using conformal radiotherapy in prostate cancer: PSA control and side effects. *Br J Cancer* 2005;92(3):488–498.

12. Peeters ST, Heemsbergen WD, Koper PC, *et al.* Dose-response in radiotherapy for localized prostate cancer: results of the Dutch multicenter randomized phase III trial comparing 68 Gy of radiotherapy with 78 Gy. *J Clin Oncol* 2006, 24(13):1990–1996.

13. Xia P, Pickett B, Vigneault E, *et al.* Forward or intensity planned segmental multileaf collimator IMRT and sequential tomotherapy to treat multiple dominant intraprostatic lesions of prostate cancer to 90 Gy. *Int. J. Radiation Oncology Biol. Phys* 2001;51:244–254.

14. Singh AK, Guion P, Sears-Crouse N, *et al.* Simultaneous integrated boost of biopsy proven, MRI defined dominant intra-prostatic lesions to 95 Gray with IMRT: early results of a phase I NCI study. *Radiation Oncology* 2007;2:36.

15. R. Shaffer, W. J. Morris, V. Moiseenko, *et al.* Volumetric Modulated Arc Therapy and Conventional Intensity-modulated Radiotherapy for Simultaneous Maximal Intraprostatic Boost: a Planning Comparison Study. *Clinical Oncology* (2009);21:401–407.

16. Pickett B, Vigneault E, Kurhanewicz J, *et al.* Static field intensity modulation to treat a dominant intra-prostatic lesion to 90 Gy compared to seven field 3-dimentsional radiotherapy. *Int. J. Radiation Oncology Biol. Phys* 1999;43:921–929.

17. Dawson LA, Litzenberg DW, Brock KK, *et al.* A comparison of ventilatory prostate movement in four treatment positions. *Int J Radiat Oncol Biol Phys* 2000;48:319–323.

18. Kitamura K, Shirato H, Seppenwoolde Y, *et al.* Three-dimensional intrafractional movement of prostate measured during real-time tumor-tracking radiotherapy in supine and prone treatment positions. *Int J Radiat Oncol Biol Phys* 2002;53:1117–1123.

19. Willoughby TR, Kupelian PA, Pouliot J, *et al.* Target localization and real-time tracking using the Calypso 4D localization system in patients with localized prostate cancer. *Int. J. Radiation Oncology Biol. Phys* 2006;65:528–534.

20. Chen H, Wu A, Brandner E. Dosimetric evaluations of the interplay effect in respiratory- gated intensity-modulated radiation therapy. *Med Phys*. 2009 Jun;36(6):2340.

21. Li H, Chetty I, Solberg T. Quantifying the interplay effect in prostate IMRT delivery using a convolution-based method. *Med Phys*. 2008 May;35(5):1703–10.

22. Schaefer M, Münter M, Thilmann C, *et al.* Influence of intra-fractional breathing movement in step-and-shoot IMRT. *Phys Med Biol*. 2004 Jun 21;49(12):N175-9.

23. Kupelian PA, Willoughby TR, Mahadevan A, *et al.* Multi-institutional clinical experience with the Calypso system in localization and continuous, real-tima monitoring of the prostate gland during external radiotherapy. *Int. J. Radiation Oncology Biol. Phys* 2007;67:1088–1098.

24. Craig T, Wong E, Bauman G, *et al.* Impact of geometric uncertainties on evaluation of treatment techniques for prostate cancer. *Int J Radiat Oncol Biol Phys* 2005;62(2):426–36.

25. Maleike D, Unkelbach J, Oelfke U. Simulation and visualization of dose uncertainties due to interfractional organ motion. *Phys Med Biol.* 2006;51(9):2237-52.

26. Hossain S, Xia P, Chuang C, *et al.* Simulated real time image guided intrafraction tracking-delivery for hypofractionated prostate IMRT.*Med Phys.* 2008;35(9):4041–8.

27. Li H, Chetty I, Enke C, *et al.* Dosimetric consequences of intrafraction prostate motion. *Int J Radiat Oncol Biol Phys*. 2008 Jul 1;71(3):801-12.

28. Chen ME, Johnston DA, Tang K, *et al.* Detailed mapping of prostate carcinoma foci: biopsy strategy implications. *Cancer* 2000;89:1800–1809.

29. Low D, Harms W, Mutic S, et al. A technique for the quantitative evaluation of dose distributions. Med. Phys. 1998 May;25(5):656–661.

30. Mohr P, Brieger S, Stahl J, *et al.* Linearity of the dose monitor system at low monitor units. *Strahlenther Onkol*. 2007 Jun;183(6):327–31.

CHAPTER 3

Discussion, Limitations and Future Work, Conclusions

3.1 Discussion

It is clear from Figure 2.3 that dose escalation to the whole prostate will likely compromise the dose received by the bladder and rectum. This observation provided the motivation to test the feasibility of escalating the dose to a DIL through different treatment techniques.

Both sequential and simultaneous IMRT and VMAT plans succeeded in escalating the dose to the DIL_PTV while keeping the bladder and rectum doses below normal tissue tolerances. However, dose escalation to the entire prostate to 86 Gy would exceed the normal tissue tolerances for the two patients.

We succeeded in delivering all the generated plans. It is clear for all the investigated plans that the treatment is less sensitive to random prostate motion than if the motion was a large sudden shift in a certain direction. In particular, VMAT sequential boost plans showed different sensitivities to motion depending on the total MU/fx delivered. VMAT has less total MU than IMRT, hence less beam on time, and generally less sensitive to patient motion. On the other hand, the low total MU/fx VMAT boost plan showed more sensitivity to motion than high total MU/fx plan for all motion patterns. Delivering too low MU per control point introduced an extra source of uncertainty. In the low MU VMAT plans for P1 and P2, their MU per degree were 0.37 and 0.39 respectively, both less than 0.5 MU per degree. This is a reason for not considering <0.5 MU per degree VMAT boost phase for treatment.

Based on the *rrms* evaluations, the loss of dose due to motion inside the DIL is least prominent for the VMAT simultaneous plan. In sequential plans, if the delivery of each plan was preceded by imaging and adjusting the patient then the motion uncertainty of the whole prostate will not provide an additional dose difference to the DIL when the whole prostate plan is delivered. This is because the field size is larger for the whole prostate plan, the DIL_PTV will totally lie within the prostate_PTV and it will receive the full prescribed dose.

The *rrms* results shown in Table 2.6 represent values for specific patterns. No statistical significance can be drawn from the differences between the average *rrms* values for the different plans. However, more analysis should be performed when considering different phases of the patterns to include a larger database from which one can analyze statistically.

The probability weighted combinations of measurements were introduced to investigate more realistically the effect of motion on the whole course of treatment. Two combinations were chosen for comparison for all the investigated plans, one that had 5 fractions of the severe motion pattern (Pattern 6) and one had 5 fractions of random motion pattern (Pattern 3). As expected the combination dominated by Pattern 3 was less sensitive to the overall motion than the combination dominated by Pattern 6.

3.2 Limitations and Future Work

One of the limitations of this work was the fact that the DIL is hypothetical and not identified by functional imaging. A future step is to apply this study to patient CT scan with an identified DIL. The DIL chosen for this study was located at the posterior-

inferior-left side of the prostate; this limited the study to one DIL location only. Inspecting the effect of the location of the DIL on the intrafractional motion is another aim for future work. It is also of interest to repeat the study on multiple DILs and inspect the limit to which a boost could be delivered without increasing the toxicity to the OARs beyond their normal tissue tolerances. The motion platform used in this work was not designed to reproduce typical motion of the prostate and a specialized motion platform that can more easily simulate the prostate intrafractional motion should be designed and built.

3.3 Conclusions

In conclusion, it is possible to escalate the dose to a DIL without exceeding normal tissue tolerances. Random motion of the prostate during treatment proved to be the least motion sensitive pattern. Sudden constant shifts in the prostate during the treatment demonstrated high degree of dose delivery errors. The impact of motion on dose delivery is sensitive to the motion phase relative to the delivery time especially if extreme motion take place at the start or end of treatment. In addition to motion uncertainty, VMAT plans with low MU per control point (e.g. less than 0.5 MU per degree) add an extra source of dose delivery uncertainty as we have seen in boost plans that were delivered over 35 fractions. The effect of motion uncertainty on the whole treatment course depends on the motion patterns taking place during treatment, this was evident when different combinations of treatment courses were compared. In conclusion, dose escalation to DIL using simultaneous boost plans with 7 mm PTV margin is feasible

in the presence of intra fractional motion, as long as the severe motion do not exceed 5 out of 35 fractions.